Supplementary Material

Force-dependent elasticity of nucleic acids

Juan Luengo-Márquez, Juan Zalvide-Pombo, Rubén Pérez and Salvatore Assenza

S1 Twistable Worm Like Chain

Here we show that the use of the twistable Worm Like Chain (tWLC) for the computation of the twist stretch coupling yields imaginary values of g for certain $\{(S, l_P)\}$ parameterizations. The explicit functional form of g from the tWLC reads[1]

$$g(f) = \pm\sqrt{SC - fC\left[\frac{x}{L_0} - 1 + \frac{1}{2}\sqrt{\frac{k_BT}{fl_P}}\right]^{-1}} \tag{S1}$$

where S and C are the stretch and twist moduli, L_0 is the equilibrium contour length, k_BT is the thermal energy, l_P is the persistence length and g is evaluated at experimentally measured $\{(x, f)\}$ points,[1] being x the extension and f the stretching force.

First note that, since g appears solely as a quadratic term in the tWLC, the solution in Eq. S1 has not a defined sign, and its choice needs to be based on complementary observations, e.g. the correlation between extension and twist. Computing a trend for $g(f)$ via the tWLC thus requires a previous notion on what is its precise behavior, so that the sign is selected accordingly.

However, as we discussed in the main text, the main problem is that certain values of S and l_P available in the literature would make the argument of the first square root in Eq. S1 negative, thus providing imaginary - and therefore unacceptable - values of $g(f)$. We show this by employing the experimental data $\{(x, f)\}$ from Ref.[1] and computing $g(f)$ over a discretized force-extension domain with approximately equal spacing between x points for stretchings ranging from 10 to 50 pN, and then computing the % of such domain that provides imaginary values of $g(f)$. We repeat such process for a range of S and l_P containing values available in the literature, and we label as *acceptable* the $\{(S, l_P)\}$ parameterizations that provide functional forms with more than 50% of the discretized domain mapping into real values of $g(f)$.

Fig. S1 (b) shows the result for $L_0 = 2.85\ \mu m$. The white region corresponds to the *acceptable* parameterizations. The red dot points the numerical fit to Eq. S1 achieved from experimental data reported in Ref.[1] It is clear that there is only a narrow range of these parameters that provides acceptable values of $g(f)$ via the tWLC. Additionally, we perform the same plot for $L_0 = 2.83\ \mu m$ (Fig. S1 a), and $L_0 = 2.87\ \mu m$ (Fig. S1 c), which evinces the noticeable sensitivity of the applicability of the tWLC model on the value of L_0.

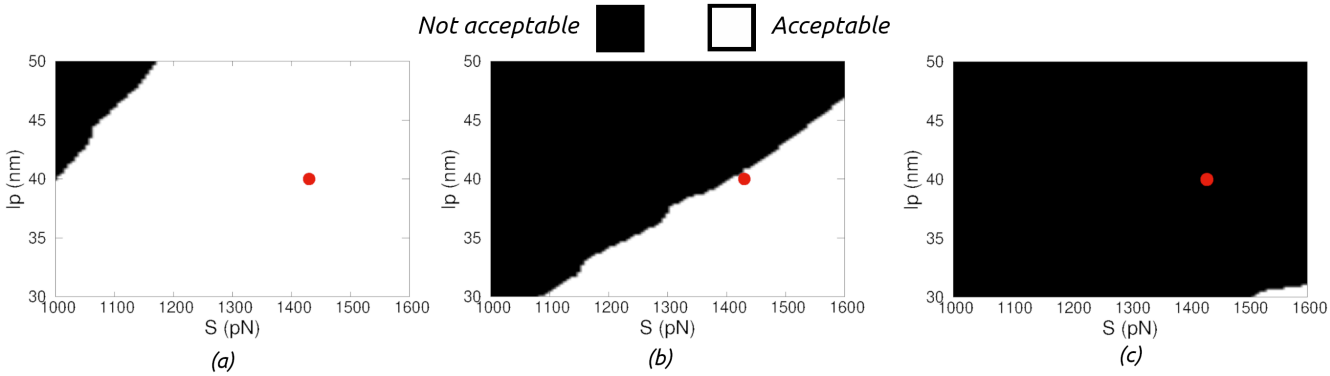

Figure S1: *Acceptable* $\{(S, l_P)\}$ parameterizations (white regions), i. e. those with more than 50 % of $\{(x, f)\}$ domain that provides real values of $g(f)$. $C = 440\ pNnm^2$ as used by *Gross et al.*[1] (a) $L_0 = 2.83\ \mu m$. (b) $L_0 = 2.85\ \mu m$, obtained from fit in *Gross et al.*,[1] with the other fitting parameters pointed out by the red dot. (c) $L_0 = 2.87\ \mu m$, the value originally used by *Gross et al.*[1] to get $g(f)$.

S2 Elastic parameters from force-extension curves

In this section, we demonstrate how the naive employment of linear fits of force-extension curves to extract the effective stretch modulus, $\widetilde{S}$, modulus would result in a systematic error on the estimated value of the force-dependent elastic parameter. Henceforth, let us call this method the Linear Fit Approach (LFA).

To illustrate this point, let $\widetilde{S}(f)$ be a monotonically non-decreasing function of f, and we apply a straightforward two points LFA, being these $(\Delta x_1, f_1, \widetilde{S}_1)$ and $(\Delta x_2, f_2, \widetilde{S}_2)$. Then $\Delta x_2 > \Delta x_1$ and $\widetilde{S}_2 \geq \widetilde{S}_1$, provided that $f_2 > f_1$.

Then, following the methodology of the LFA, we have that the effective stretch modulus estimated this way would be

$$\widetilde{S}_{LFA} = \frac{L_0(f_2 - f_1)}{< \Delta x_2 > - < \Delta x_1 >} = \frac{\widetilde{S}_1 \widetilde{S}_2 (f_2 - f_1)}{f_2 \widetilde{S}_1 - f_1 \widetilde{S}_2}$$

As $\widetilde{S}_1 > 0$, $\widetilde{S}_2 > 0$, $\widetilde{S}_{LFA} > 0$ and $f_2 > f_1$, the denominator $f_2 \widetilde{S}_1 - f_1 \widetilde{S}_2$ must also be larger than zero. The previous may be rearranged as

$$\frac{\widetilde{S}_{LFA}}{\widetilde{S}_2} = 1 + \frac{f_1(\widetilde{S}_2 - \widetilde{S}_1)}{f_2 \widetilde{S}_1 - f_1 \widetilde{S}_2} \tag{S2}$$

which must be larger or equal to 1 by the hand of the preceding arguments. This results in $\widetilde{S}_{LFA} \geq \widetilde{S}_2 \geq \widetilde{S}_1$, meaning that for a monotonically non-decreasing $\widetilde{S}(f)$, the effective stretch modulus measured through the LFA is larger or equal than the largest value of $\widetilde{S}(f)$ within the force domain at which we measure $< \Delta x >$. The argument can be adapted straightforwardly to the case of non-increasing $\widetilde{S}(f)$, which would lead to an underestimation of the elastic constant.

S3 Force-dependent fluctuations approach

In this section, we provide a detailed derivation of the equation that relates the fluctuations of the deformation modes with the elastic parameters of the model.

As indicated in the main text, the Elastic Rod Model (ERM) comprises an energy composed of second order monomials of the deformation modes, where the leading coefficients are the elastic parameters of the model. If we denote every deformation mode by integers $i,\ j \in \{1, 2, 3, ..., N\}$, being N the total number of deformation modes, then we can write the ERM energy as

$$E(\bar{\boldsymbol{q}}) = \frac{1}{2}\sum_{i}^{N}\sum_{j}^{N} k_{ij}\Delta q_i \Delta q_j - \sum_{i}\gamma_i \Delta q_i \tag{S3}$$

Being $\bar{\boldsymbol{q}} = (q_1, q_2, ..., q_N)$, so that the energy is a function of the coordinates q_i. Besides, k_{ij} are the elastic parameters. If $i = j$, we call k_{ii} the *elastic modulus of the deformation mode* i. On the contrary, if $i \neq j$, we call $\frac{1}{2}(k_{ij} + k_{ji})$ the *coupling term between the deformation modes* i and j.

In Eq. S3, γ_i represents a generalized mechanical stress applied to the deformation mode i, while Δq_i is the difference of a quantity assigned to the deformation mode and its equilibrium value. This equilibrium value is taken as the conformational average of that measure of the deformation mode in the absence of mechanical stresses.

The derivative of $E(\bar{\boldsymbol{q}})$ in Eq. S3 with respect to an arbitrary coordinate q_β yields

$$\frac{\partial E(\bar{\boldsymbol{q}})}{\partial q_\beta} = \frac{1}{2}\sum_{i}^{N}(k_{i\beta} + k_{\beta i})\Delta q_i - \gamma_\beta \tag{S4}$$

We then proceed by taking the mean value of Eq. S4 times an arbitrary coordinate Δq_α. The mean value of the right hand equals $\delta_{\alpha\beta}k_BT$, courtesy of the generalized equipartition theorem

$$\left\langle q_\alpha \frac{\partial E(\bar{\boldsymbol{q}})}{\partial q_\beta} \right\rangle = \delta_{\alpha\beta}k_BT \tag{S5}$$

where k_BT is the thermal energy of the system and $\delta_{\alpha\beta}$ is the Kronecker delta. We rearrange properly the resulting expression to achieve

$$\left\langle \Delta q_\alpha \frac{\partial E(\bar{\boldsymbol{q}})}{\partial q_\beta} \right\rangle = \frac{1}{2}\left[\sum_{i}^{N}\langle \Delta q_\alpha \Delta q_i\rangle\, k_{i\beta} + \sum_{i}^{N} k_{\beta i}\langle \Delta q_i \Delta q_\alpha\rangle\right] - \langle \Delta q_\alpha\rangle\,\gamma_\beta = \delta_{\alpha\beta}k_BT \tag{S6}$$

This ordering is possible since $\langle \Delta q_\alpha \Delta q_i\rangle = \langle \Delta q_i \Delta q_\alpha\rangle$. Let us now do the following definitions

$$\left[\bar{\bar{\boldsymbol{\Gamma}}}\right]_{ij} = \langle \Delta q_i\rangle\,\gamma_j$$

$$\left[\bar{\bar{\boldsymbol{V}}}\right]_{ij} = \langle \Delta q_i \Delta q_j\rangle$$

$$\left[\bar{\bar{\boldsymbol{\Lambda}}}\right]_{ij} = k_{ij}$$

By virtue of these, the information contained in Eq. S6 may be compacted as

$$\frac{1}{2}\left[\bar{\bar{\boldsymbol{V}}}\bar{\bar{\boldsymbol{\Lambda}}} + \left(\bar{\bar{\boldsymbol{\Lambda}}}\bar{\bar{\boldsymbol{V}}}\right)^T\right] - \bar{\bar{\boldsymbol{\Gamma}}} = k_BT\bar{\bar{\boldsymbol{I}}} \tag{S7}$$

With $\bar{\bar{\boldsymbol{I}}}$ as the $N \times N$ identity matrix. Taking into account that $\left(\bar{\bar{\boldsymbol{\Lambda}}}\bar{\bar{\boldsymbol{V}}}\right)^T = \left(\bar{\bar{\boldsymbol{V}}}\right)^T \left(\bar{\bar{\boldsymbol{\Lambda}}}\right)^T$ and adding $\bar{\bar{\boldsymbol{\Gamma}}}$ to both sides, we have

$$\frac{1}{2}\left[\bar{\bar{\boldsymbol{V}}}\bar{\bar{\boldsymbol{\Lambda}}} + \left(\bar{\bar{\boldsymbol{V}}}\right)^T \left(\bar{\bar{\boldsymbol{\Lambda}}}\right)^T\right] = k_B T \bar{\bar{\boldsymbol{I}}} + \bar{\bar{\boldsymbol{\Gamma}}} \tag{S8}$$

But we know that the covariance matrix $\bar{\bar{\boldsymbol{V}}}$ is symmetric, and therefore $\left(\bar{\bar{\boldsymbol{V}}}\right)^T = \bar{\bar{\boldsymbol{V}}}$. The final result is reached by multiplying from the left side by $\left(\bar{\bar{\boldsymbol{V}}}\right)^{-1}$, and defining the stiffness matrix as $\bar{\bar{\boldsymbol{K}}} = \frac{1}{2}\left[\bar{\bar{\boldsymbol{\Lambda}}} + \left(\bar{\bar{\boldsymbol{\Lambda}}}\right)^T\right]$

$$\bar{\bar{\boldsymbol{K}}} = \left(\bar{\bar{\boldsymbol{V}}}\right)^{-1}\left(k_B T \bar{\bar{\boldsymbol{I}}} + \bar{\bar{\boldsymbol{\Gamma}}}\right) \tag{S9}$$

One observation is worth mentioning. On one hand, $\left[\bar{\bar{\boldsymbol{K}}}\right]_{ij} = \left[\bar{\bar{\boldsymbol{K}}}\right]_{ji}$ by construction. However, the right-hand side of Eq. S9 is not necessarily symmetric.

Whether that relation holds or not depends on the physics of the problem. However, as mathematically it is true that the left-handed matrix is symmetric, this imposes constraints of the type $\delta\left(\left[\bar{\bar{\boldsymbol{M}}}\right]_{ij} - \left[\bar{\bar{\boldsymbol{M}}}\right]_{ji}\right)$, for $i \neq j$, being $\bar{\bar{\boldsymbol{M}}}$ the result of operating the right-hand side of Eq. S9.

There are as many of these constraints as pairs of deformation modes, and their fulfillment points out the adequacy of the ERM to describe the physics of that specific system. As we discuss below, a system that follows purely the energy of the ERM will always satisfy these constraints.

In this regard, let us consider a system whose mechanics can be completely characterized by only two degrees of freedom: stretching and torsion. The corresponding mechanical stresses exerted on these deformation modes could be a force and a torque, respectively, but we restrict ourselves to the case when there is no applied torque. The ERM energy of a stretched chain reads

$$E(L,\theta) = \frac{1}{2}\frac{S}{L_0}\Delta L^2 + \frac{1}{2}\frac{C}{L_0}\Delta\theta^2 + \frac{g}{L_0}\Delta L\Delta\theta - \Delta L f \tag{S10}$$

Where $\Delta L = L - L_0$, and $\Delta\theta = \theta - \theta_0$ describe a conformation of the chain deformed at force f. Note also that $L = L(f)$, $\theta = \theta(f)$ and $L_0 = \langle L(f=0)\rangle$, $\theta_0 = \langle\theta(f=0)\rangle$, where $\langle ...\rangle$ denotes the conformational average.

For $N = 2$, we can write Eq. S9 following the notation in Eq. S10, as

$$\frac{1}{L_0}\begin{pmatrix} S & g_{12} \\ g_{21} & C \end{pmatrix} = \left[\begin{pmatrix} \langle\Delta L^2\rangle & \langle\Delta L\Delta\theta\rangle \\ \langle\Delta L\Delta\theta\rangle & \langle\Delta\theta^2\rangle \end{pmatrix}\right]^{-1}\left[k_B T\begin{pmatrix} 1 & 0 \\ 0 & 1 \end{pmatrix} + \begin{pmatrix} \langle\Delta L\rangle f & 0 \\ \langle\Delta\theta\rangle f & 0 \end{pmatrix}\right] \tag{S11}$$

By virtue of the symmetry of the stiffness matrix, there is a constraint with the form $\delta(g_{12} - g_{21})$. Nevertheless, as the solution of Eq. S11 yields mathematically different expressions for both, we maintain this notation in order to distinguish the two solutions of the twist-stretch coupling. After working out Eq. S11 we achieve

$$\frac{S}{L_0} = \frac{1}{|\bar{\bar{\boldsymbol{V}}}|}(k_B T\left\langle\Delta\theta^2\right\rangle - f[\langle\Delta L\Delta\theta\rangle\langle\Delta\theta\rangle - \left\langle\Delta\theta^2\right\rangle\langle\Delta L\rangle])$$

$$\frac{C}{L_0} = \frac{1}{|\bar{\bar{\boldsymbol{V}}}|} k_B T \left\langle \Delta L^2 \right\rangle$$

$$\frac{g_{12}}{L_0} = -\frac{1}{|\bar{\bar{\boldsymbol{V}}}|} k_B T \left\langle \Delta L \Delta\theta \right\rangle$$

$$\frac{g_{21}}{L_0} = -\frac{1}{|\bar{\bar{\boldsymbol{V}}}|} (k_B T \left\langle \Delta L \Delta\theta \right\rangle - f[\left\langle \Delta L^2 \right\rangle \left\langle \Delta\theta \right\rangle - \left\langle \Delta L \right\rangle \left\langle \Delta L \Delta\theta \right\rangle])$$

where $|\bar{\bar{\boldsymbol{V}}}| = \left\langle \Delta L^2 \right\rangle \left\langle \Delta\theta^2 \right\rangle - \left\langle \Delta L \Delta\theta \right\rangle^2$.

We further define the function

$$\Delta(f) = \frac{2(g_{12} - g_{21})}{g_{12} + g_{21}} = \frac{2f(\left\langle \Delta L \right\rangle \left\langle \Delta L \Delta\theta \right\rangle - \left\langle \Delta L^2 \right\rangle \left\langle \Delta\theta \right\rangle)}{|\bar{\bar{\boldsymbol{V}}}|(g_{12} + g_{21})} \tag{S12}$$

as an adimensional measure of the insufficiency of the ERM to describe the system.

Clearly, $\Delta(0) = 0$. Therefore, in the absence of a force, the constraint is trivially fulfilled. In general, in the absence of any deformation stress, the right hand of equation S9 is symmetric and the well-known result of the fluctuations approach for the unperturbed ERM is recovered.

In order to show that a system purely described by Eq. S10 will trivially satisfy the constraint in Eq. S12, we run a Monte Carlo (MC) simulation where the Metropolis algorithm is applied directly over the energy of the ERM, and the proposed MC moves are obtained by picking randomly ΔL and $\Delta\theta$ with step lengths chosen with uniform probability from a $[-0.2, 0.2]$ interval.

For five different forces, we solve the elastic parameters from Eq. S11, and the constraint $\Delta(f)$ from Eq. S12. The results for each force are averaged throughout 10 independent realizations. Every realization is composed of 10^7 Monte Carlo steps, and the first 20% of them are rejected, while only one every ten of the subsequent realizations is taken into account for statistics. The acceptance ratio is fixed to be approximately 0.56 in all realizations.

Fig. S2 displays the results, showing that the fluctuations approach gives at all forces a correct result within error. The expected output - fixed a priori in the code and consistent with dsDNA elastic parameters taken from the literature - is indicated with a red line in every figure.

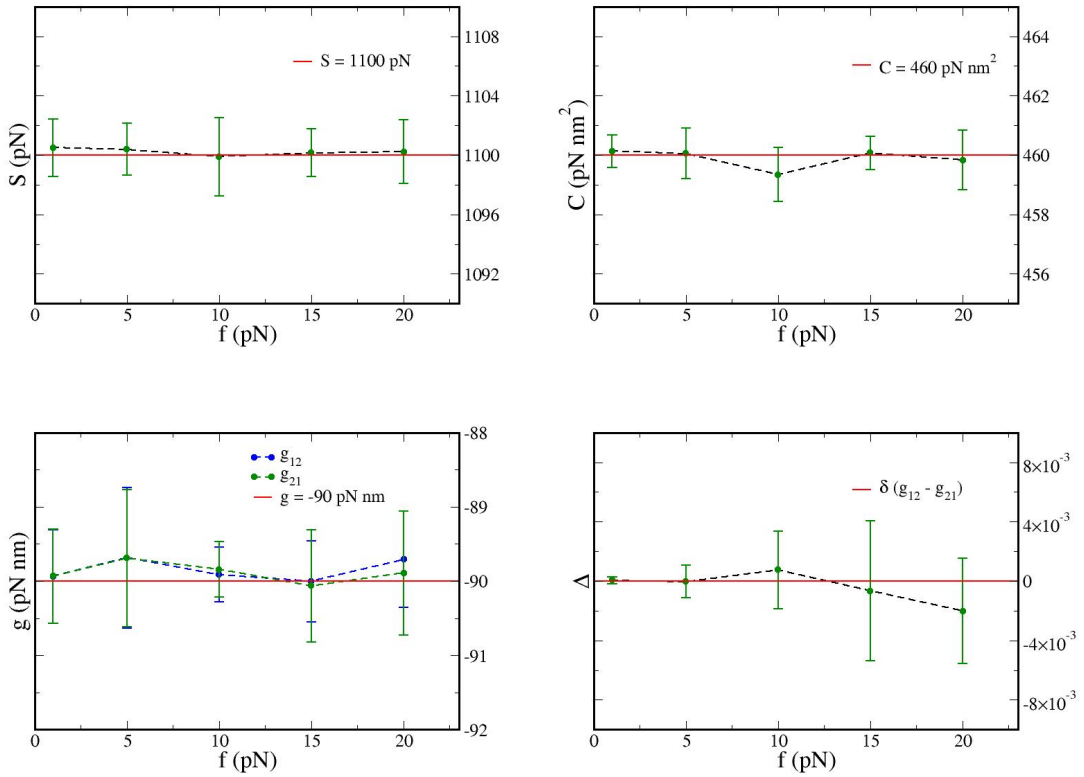

Figure S2: Elastic parameters and constraint for several forces, computed with the force-dependent fluctuations approach proposed in this work applied to data arising from a MC simulation of the energy of the stretched ERM.

S4 Application to stretched dsDNA and dsRNA

S4.1 All-atom MD simulations

Table S1 and S2 report, for dsDNA and dsRNA respectively, the list of sequences analyzed with the approach introduced in the present study,[2,5,6] together with the label assigned to each sequence for the subsequent representation of the elastic parameters.

The sequences are displayed from the 5' end to the 3' end in all cases. The fragments on the left and right of the hyphens are handles that have not been considered for the analysis, and whose purpose is to avoid end-effects.

In Section S5 we display the set of elastic parameters for each of the tabulated sequences and its dependence on the stretching force, as obtained from the application of Eq. S11. The error bars were estimated by splitting the data in 5 blocks, computing the elastic constants in each of them, and then applying the bootstrap method.[8]

In order to describe the sequence-dependent curvature of each molecule, we use the crookedness, β, as the characteristic parameter of every sequence. The crookedness is defined as

$$\beta(f) = \arccos\left(\frac{L(f)}{\sum_i d_i(f)}\right) \tag{S13}$$

Being $L(f)$ the contour length of the molecule axis computed as the sum of the helical rises of all steps, and d_i the Euclidean distance between the centers of the two consecutive basepairs belonging to the step i. This magnitude is proportional to the displacement of

Label	Sequence
A4GGA4	CGCG-AAAAGGAAAA-CGCG
A4TA4	CGCG-AAAATAAAA-CGCG
A8GG	CGCG-AAAAAAAAGG-CGCG
A8T	CGCG-AAAAAAAAT-CGCG
DDD	CGCG-CGCGAATTCGCG-CGCG
DNAall	GCG-CAATGGAGTA-CGC
DUE	CGCG-GATCTATTTATTT-CGCG
G4AAG4	CGCG-GGGGAAGGGG-CGCG
G4CG4	CGCG-GGGGCGGGG-CGCG
PolyA	CGCG-AAAAAAAAAA-CGCG
PolyAC	CGCG-ACACACACAC-CGCG
PolyAG	CGCG-AGAGAGAGAG-CGCG
PolyAT	CGCG-ATATATATAT-CGCG
PolyCG	CGCG-CGCGCGCGCG-CGCG
PolyG	CGCG-GGGGGGGGGG-CGCG
TATA	CGCG-CGCGAATTCGCG-CGCG
TFBS	CGCG-CGCGAATTCGCG-CGCG

Table S1: Sequences of dsDNA analyzed in this work

Label	Sequence
AA	GGGG-AAAAAAAAAAAAAAAA-GGGG
AC	GGGG-ACACACACACACACAC-GGGG
AG	GGGG-AGAGAGAGAGAGAGAG-GGGG
AU	GGGG-AUAUAUAUAUAUAUAU-GGGG
CG	GGGG-CGCGCGCGCGCGCGCG-GGGG
GG	GGGG-GGGGGGGGGGGGGGGG-GGGG
seq1	GGGG-CCUAACAUCGAUUCGC-GGGG
seq2	GGGG-UACUGCACUAACGCGA-GGGG
seq3	GGGG-CCGGUAGCCAGGCCGU-GGGG
seq4	GGGG-AUCUUAAUGAAUCAGA-GGGG
RNAall	GCG-CAAUGGAGUA-CGC

Table S2: Sequences of dsRNA analyzed in this work

the basepairs composing the chain with respect to the axis of the molecule.

The constraint function defined in Eq. S12 is presented in the Section S5 in addition to the elastic parameters. It may be understood as a measure of the insufficiency of the perfectly straight ERM to describe satisfactorily the elastic properties of nucleic acids with a certain intrinsic curvature. This is evinced by realizing the correlation between the slope of $\Delta(f)$ with $\beta(f = 1\ pN)$ for all dsDNA sequences, as displayed in Fig S3.

The obvious correlation displayed for the dsDNA molecule sets the variation in the constraint as an indicator that the ERM does not provide a completely satisfactory description of the deformability of the chain. This happens because a molecule with large intrinsic crookedness will respond to an external perturbation through some deformation modes that are not properly considered by the ERM as it is written in Eq. S10.

In the case of dsRNA sequences, the previous correlation is far from being clear, but this is ascribed to the fact that the dsRNA intrinsic crookedness is much larger and its value

for the different sequences is spread along a smaller range.

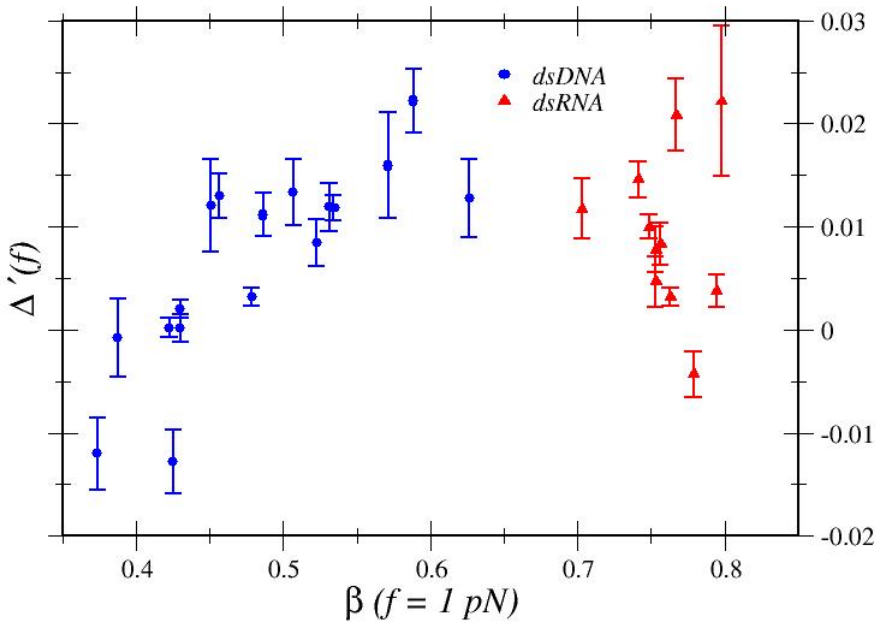

Figure S3: Slope of $\Delta(f)$ versus $\beta(f = 1pN)$ for dsDNA (blue circles) and dsRNA (red triangles). The computation of the slope entails the assumption that $\Delta(f)$ is approximately linear in f, which is not always true, but allows simpler conveyance of the information gathered by the analysis. The error bars are the standard errors of the slopes.

S4.2 Equivalence between crookedness and bending angle

In this section, we show that for a regular helix the definition of the crookedness matches the one of the helix angle. Let us name in this section the crookedness as β and the helix angle as ϕ. We thus aim at proving that $\beta = \phi$. From the definition of ϕ, it is clear that

$$\tan(\phi) = r\omega \tag{S14}$$

being r the radius of the helix and $\omega = \frac{2\pi}{P}$ the helical frequency, where P is the helical pitch. The equation of the helix is

$$\vec{R}(z) = r\cos(\omega z)\hat{i} + r\sin(\omega z)\hat{j} + z\hat{k} \tag{S15}$$

The contour length is thus computed as

$$L = \int_0^h \left| \frac{d\vec{R}(z)}{dz} \right| dz = h\sqrt{1 + (r\omega)^2} \tag{S16}$$

Where h is the helical rise. For a system composed of a single step, the crookedness reads

$$\cos(\beta) = \frac{h}{L} = \frac{1}{\sqrt{1 + (r\omega)^2}}$$

Where for the last step the relation in Eq. S16 was used. Since $\cos(\alpha) = \frac{1}{\sqrt{1+\tan^2(\alpha)}}$, comparing the former and Eq. S14, we conclude that indeed $\beta = \phi$.

S4.3 Toy Model for the variation of the Twist Modulus

In this section we make explicit the derivation of Eq. 4 of the main text. From the origin of the coordinate frame $\vec{P}_0 \coloneqq (0,0,0)$, we set three pairs of points representing three base-pairs

$$\vec{A}_0 \coloneqq \vec{P}_0 - r\hat{y}, \quad \vec{B}_0 \coloneqq \vec{P}_0 + r\hat{y}$$
$$\vec{A}_1 \coloneqq \bar{\bar{R}}_{xy}(-\theta)\vec{A}_0 + b\hat{z}, \quad \vec{B}_1 \coloneqq \bar{\bar{R}}_{xy}(-\theta)\vec{B}_0 + b\hat{z}$$
$$\vec{A}_2 \coloneqq \bar{\bar{R}}_{xy}(-\theta)\vec{A}_1 + b\hat{z} = \bar{\bar{R}}_{xy}(-2\theta)\vec{A}_0 + 2b\hat{z}, \quad \vec{B}_2 \coloneqq \bar{\bar{R}}_{xy}(-\theta)\vec{B}_1 + b\hat{z} = \bar{\bar{R}}_{xy}(-2\theta)\vec{B}_0 + 2b\hat{z}$$

Whence $r, b \in \mathbb{R}^+$, θ is the intrinsic torsion angle, and the rotation matrix in the xy plane is

$$\bar{\bar{R}}_{xy}(\phi) = \begin{pmatrix} \cos(\phi) & -\sin(\phi) & 0 \\ \sin(\phi) & \cos(\phi) & 0 \\ 0 & 0 & 1 \end{pmatrix}$$

We now define $\vec{P}_1 \coloneqq \vec{P}_0 + b\hat{z}$, and $\vec{P}_2 \coloneqq \vec{P}_1 + b\hat{z}$. We next rotate counterclockwise in the yz plane the points $\vec{A}_2$ and $\vec{B}_2$ from $\vec{P}_1$ by a bending angle β to define

$$r_\beta(\vec{A}_2) \coloneqq \bar{\bar{R}}_{yz}(-\beta)\left[\vec{A}_2 - \vec{P}_1\right], \quad r_\beta(\vec{B}_2) \coloneqq \bar{\bar{R}}_{yz}(-\beta)\left[\vec{B}_2 - \vec{P}_1\right]$$

Being the rotation matrix in the yz plane

$$\bar{\bar{R}}_{yz}(\phi) = \begin{pmatrix} 1 & 0 & 0 \\ 0 & \cos(\phi) & -\sin(\phi) \\ 0 & \sin(\phi) & \cos(\phi) \end{pmatrix}$$

If we further define $r_\beta(\vec{P}_2) = \bar{\bar{R}}_{yz}(-\beta)\left[\vec{P}_2 - \vec{P}_1\right]$, it is easy to show that $\vec{P}_i = [\vec{A}_i + \vec{B}_i]/2$ $\forall i \in \{0,1,2\}$, and that $r_\beta(\vec{P}_2) = [r_\beta(\vec{A}_2) + r_\beta(\vec{B}_2)]/2$. Then $\vec{P}_0$, $\vec{P}_1$ and $r_\beta(\vec{P}_2)$ represent the centers of the base-pairs in this toy model. We assign to each center a vector pointing from one base to the opposite one defined as $\vec{u}_i = \vec{B}_i - \vec{A}_i$ $\forall i \in \{0,1,2\}$, and $r_\beta(\vec{u}_2) = r_\beta(\vec{B}_2) - r_\beta(\vec{A}_2)$. It is also straightforward to show that $|\vec{u}_0| = 2r$, and since the rest are obtained through isometries of the space from $\vec{u}_0$, it must be $|\vec{u}_i| = 2r$ $\forall i \in \{0,1,2\}$, together with $|r_\beta(\vec{u}_2)| = 2r$.

The torsion angle $\chi(\theta,\beta)$ is the one formed between the projections on the xy plane of $\vec{u}_1$ and $r_\beta(\vec{u}_2)$, whose versors are denoted as $\hat{u}_{1,xy}$ and $\hat{r}_\beta(u_2)_{xy}$ respectively. This amounts to

$$\chi(\theta,\beta) = \arccos\left[\hat{u}_{1,xy} \cdot \hat{r}_\beta(u_2)_{xy}\right] = \arccos\left\{ \cos(\theta)\left[\frac{\cos(\beta) + 2\sin^2(\theta)(1-\cos(\beta))}{\sqrt{1-\cos^2(2\theta)\sin^2(\beta)}}\right]\right\} \tag{S17}$$

The schematic representation of the toy model is shown in Fig. S4. We next assume that the intrinsic torsion angle θ is a random variable following a Boltzmann distribution of an energy that is harmonic on the torsional deformability. The variance is $\langle \Delta\theta^2 \rangle = L_0 k_B T/\widetilde{C}$, as given by the equipartition theorem, with a constant intrinsic twist modulus $\widetilde{C}$. Analogously, the twist modulus, $C(\beta)$ is related to the variance of the torsion angle via $C(\beta) = L_0 k_B T / \langle \Delta\chi(\theta,\beta)^2 \rangle$. For small variations of β around β_0, we can perform the expansion

$$C(\beta) \approx C(\beta_0) + \left(\frac{\partial C(\beta)}{\partial \beta}\right)_{\beta=\beta_0} (\beta - \beta_0) \tag{S18}$$

$$\left(\frac{\partial C(\beta)}{\partial \beta}\right)_{\beta=\beta_0} = -L_0 k_B T \left[\frac{1}{\langle \Delta\chi(\theta,\beta_0)^2 \rangle^2}\left(\frac{\partial \langle \Delta\chi(\theta,\beta)^2 \rangle}{\partial \beta}\right)_{\beta=\beta_0}\right]$$

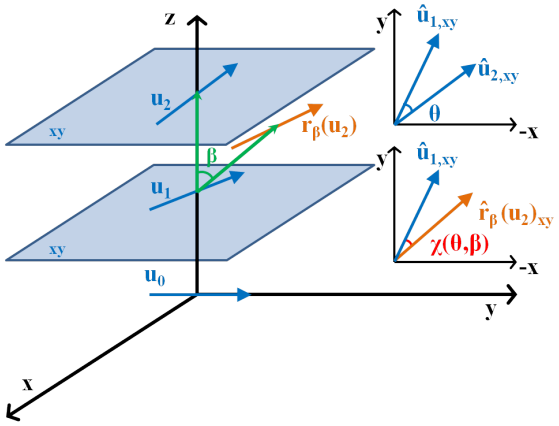

Figure S4: Elements of the Toy Model. The torsion angle $\chi(\theta, \beta)$ will be the one formed by the projection on the xy plane of the rotation by an angle β of the top vector with the adjacent vector.

where the brackets denote the ensemble average over θ. Indeed, being $\chi(\theta, \beta)$ a function of a single random variable, by the Law Of The Unconscious Statistician (LOTUS) we can use the probability distribution of θ to compute any expected value of a function of $\chi(\theta, \beta)$. For further simplifications, we assume that $\chi(\theta, \beta)$ and its derivative with respect to β are approximately linear around the statistically significant variations of θ around θ_0, which is equivalent to state that $\widetilde{C}/L_0 k_B T \gg 1$, so that

$$\chi(\theta, \beta_0) \approx g_0 + g_1[\theta - \theta_0], \quad g_0 = \chi(\theta_0, \beta_0), \; g_1 = \left(\frac{\partial \chi(\theta, \beta_0)}{\partial \theta}\right)_{\theta=\theta_0}$$

$$\left(\frac{\partial \chi(\theta, \beta)}{\partial \beta}\right)_{\beta=\beta_0} \approx h_0 + h_1[\theta - \theta_0], \quad h_0 = \left(\frac{\partial \chi(\theta_0, \beta)}{\partial \beta}\right)_{\beta=\beta_0}, \; h_1 = \left[\frac{\partial}{\partial \theta}\left(\frac{\partial \chi(\theta, \beta_0)}{\partial \beta}\right)_{\beta=\beta_0}\right]_{\theta=\theta_0}$$

where we have omitted the fact that g_0, g_1, h_0 and h_1 are all functions of θ_0 and β_0 in order to simplify the notation. Employing the previous expansions and by the hand of the LOTUS, we can now compute

$$\left\langle \Delta\chi(\theta, \beta_0)^2 \right\rangle = \int_{-\infty}^{\infty} P(\theta)[\chi(\theta, \beta_0) - g_0]^2 d\theta \approx g_1^2 \frac{L_0 k_B T}{\widetilde{C}} \tag{S19}$$

$$\left(\frac{\partial \left\langle \Delta\chi(\theta, \beta)^2 \right\rangle}{\partial \beta}\right)_{\beta=\beta_0} = \int_{-\infty}^{\infty} P(\theta) 2[\chi(\theta, \beta_0) - g_0] \left(\frac{\partial \chi(\theta, \beta)}{\partial \beta}\right)_{\beta=\beta_0} d\theta \approx g_1 h_1 \frac{2 L_0 k_B T}{\widetilde{C}} \tag{S20}$$

being $P(\theta)$ the probability distribution function of θ. The result sketched in Eq. S19 also relates the intrinsic twist modulus with the twist modulus at zero force: $\widetilde{C} = g_1^2 C(\beta_0)$. We continue by substituting Eq. S19 and S20 in Eq. S18, and making use of the relation between $\widetilde{C}$ and $C(\beta_0)$ to achieve

$$C(\beta) = C(\beta_0)\left[1 + \sin(\beta_0)\Omega(\theta_0, \beta_0)\,(\beta - \beta_0)\right] \tag{S21}$$

$$\Omega(\theta, \beta) = \frac{16\left[3\cos(4\theta) - 1 + \cos(2\beta)\{1 + \cos(4\theta)\}\right]}{\left[\cos(4\theta) - 3 - \cos(2\beta)\{1 + \cos(4\theta)\}\right]\left[8\cos(\beta) + \cos(4\theta) - 3 - \cos(2\beta)\{1 + \cos(4\theta)\}\right]}$$

Which is Eq. 4 of the main text. We shall recall here that, as discussed in the main text, the expansion performed to achieve Eq. S21 is accurate in the limit $\widetilde{C}/L_0 k_\beta T \to \infty$, when the fluctuations of the intrinsic torsion angle are small.

Fig. S5 displays the crookedness stiffnesses computed for all dsDNA and dsRNA sequences from its definition $\partial \cos(\beta)/\partial f = \cos(\beta_0)/k_\beta$ via linear regression assuming linearity versus the corresponding crookedness at 1 pN. The error bars are the standard deviations computed through error propagation neglecting the covariance term. We observe that the fit presented in Ref.[2] reproduces satisfactorily the trend for both dsDNA and dsRNA. Finally, Fig S6 represents the relative variation of the twist modulus $C'(f)/C(\beta_0)$ against

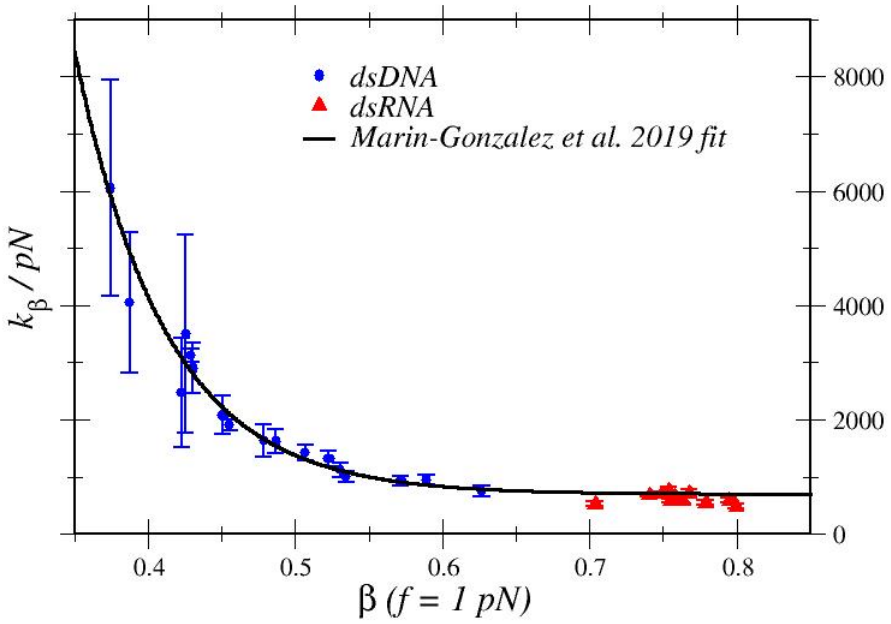

Figure S5: Crookedness stiffness, k_β, as a function of the intrinsic crookedness, $\beta(f = 1pN)$ for the dsDNA sequences (blue circles) and the dsRNA sequences (red triangles) analyzed in this work. The black solid line represents the fit performed by Marin-Gonzalez *et al.*[2] and used for the analytic result in Fig. 1 center of the main text.

the intrinsic crookedness for both the simulation analysis and the analytical solution of the model that we have described. We also display the numerical solution of the model in order to show under which conditions is the analytic approximation reliable.

Solving numerically the model requires as additional input the intrinsic twist modulus $\widetilde{C}$ and the contour length. The former is expected to depend on the specific sequence, and the latter is not the same for all molecules studied in this work, so we choose to show two representative cases. We display the dsDNA numerical solution with $\widetilde{C} = 435\ pN\ nm^2$ and $L_0 = 9 \times 0.34\ nm$, where the twist modulus has been taken from Ref.,[3] and we compute the contour length as the number of steps of PolyA times the typical helical rise of a dsDNA step.

On the other hand, the dsRNA numerical solution is computed with $\widetilde{C} = 410\ pN\ nm^2$ and $L_0 = 15 \times 0.28\ nm$, being both $\widetilde{C}$ and the helical rise taken from Ref.,[4] and where 15 is the number of bp steps of most dsRNA sequences analyzed in this work. Moreover, we display a numerical solution with L_0 of dsDNA and twice its twist modulus in order to show that indeed for large $\widetilde{C}$ the numerical solution matches the analytical result.

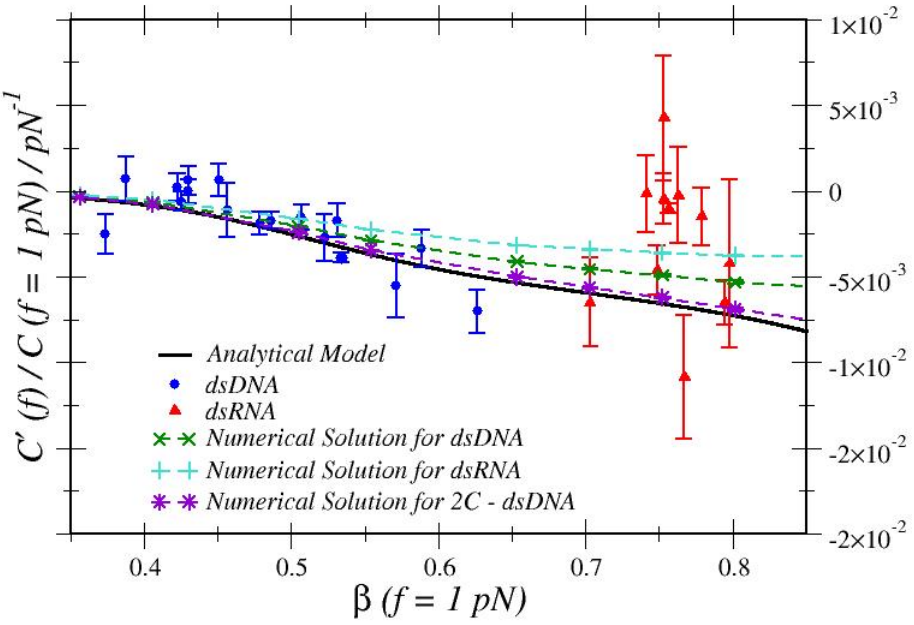

Figure S6: Relative variation of the twist modulus, $C'(f)/C(\beta_0)$, as a function of the intrinsic crookedness, $\beta(f = 1pN)$, for the dsDNA sequences (blue circles), the dsRNA sequences (red triangles), and the analytic result for the Toy Model (black solid line). Green crosses correspond to the numerical solution with dsDNA input, cyan plusses correspond to the numerical solution with dsRNA input, and violet stars correspond to the numerical solution with twice the twist modulus of dsDNA.

S4.4 Variation of the Stretch Modulus

Here we detail the interpretation of the variation of the stretch modulus in terms of the model presented in Ref.,[2] which states that the stretch modulus may be expressed as

$$\frac{1}{S(f)} = \sum_i \frac{1}{k_{l,i}} + \frac{1}{k_\beta(f)}$$

Being $k_{l,i}$ the stiffness constant assigned to the base-pair step i, and $k_\beta(f)$ the force-dependent crookedness stiffness. If we account for the crooked curvature, the complete energy of the system can be written as

$$E(L,\theta,\beta) = E_{ERM}(L,\theta) + L_0 \frac{k_\beta}{2\cos(\beta_0)}[\cos(\beta(f)) - \cos(\beta_0)]^2 - L_0 f[\cos(\beta(f)) - \cos(\beta_0)]$$

where $E_{ERM}(L,\theta)$ is the energy in Eq. S10 and $\beta_0 =< \beta(f = 0) >$. Now, taking advantage of the fact that the deformation of the crooked curvature is decoupled with respect to the remaining deformation modes in this expression, we use the generalized equipartition theorem to reach

$$k_\beta(f) = \cos(\beta_0) \frac{k_B T + f L_0 \Big\langle [\cos(\beta(f)) - \cos(\beta_0)] \Big\rangle}{L_0 \Big\langle [\cos(\beta(f)) - \cos(\beta_0)]^2 \Big\rangle} \tag{S22}$$

being $k_B T$ the thermal energy of the system. We compute $k_\beta(f)$ from Eq. S22 for all the sequences studied in this work. In order to compact the sign and magnitude of the

dependence of $k_\beta(f)$ on f, we follow the same strategy suggested for the elastic parameters, meaning that we perform linear regressions of $k_\beta(f)$ versus force representations, and express $k'_\beta(f)$ as the slope of such regression, with the standard error of the slope giving an idea of how much does the habit of $k_\beta(f)$ deviates from linearity.

Fig. S7 shows the resulting $k'_\beta(f)$ with respect to the relative slide variation. First to

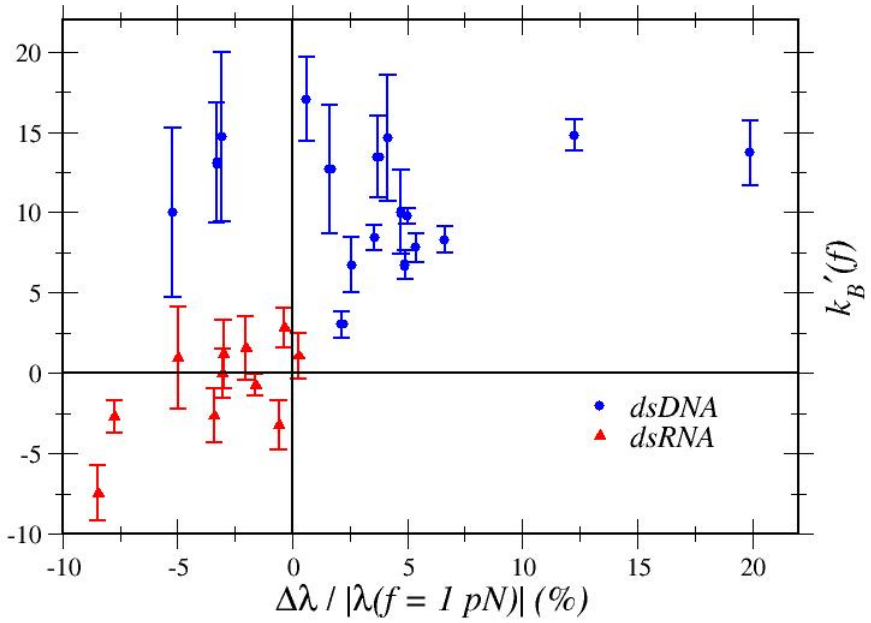

Figure S7: Slopes of Crookedness stiffnesses versus force representations as a function of the relative slide variation for all dsDNA sequences (blue circles) and all dsRNA sequences (red triangles) analyzed in this work.

notice is that, as expected from the discussion in the main text, $k'_\beta(f) > 0$ for all dsDNA sequences, and $k'_\beta(f) < 0$ within error for most dsRNA sequences.

Additionally, we observe that with the exception of a few dsDNA sequences, the set displays a positive correlation between $k'_\beta(f)$ and the relative slide variation, which is consistent with our hypothesis that the change of the stretch modulus should be ascribed to a change in this parameter, and the subsequent change of the strength of the stacking interactions.

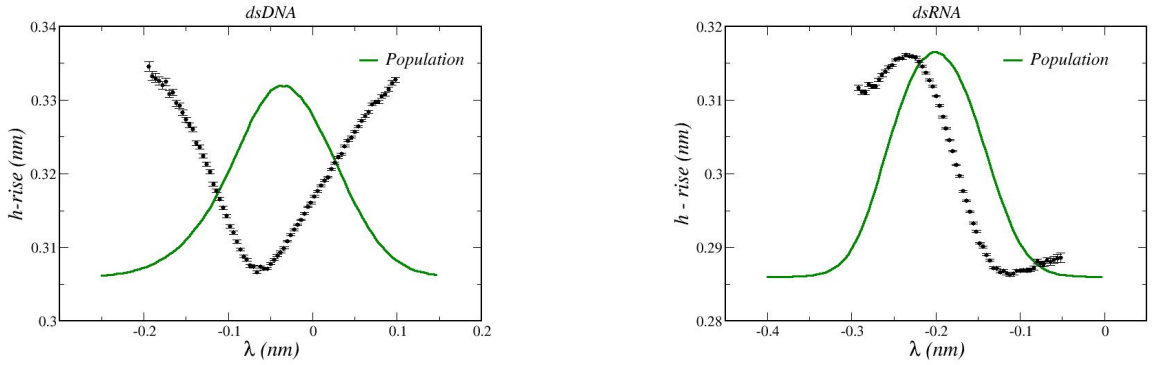

(a) (b)

Figure S8: h-rise against slide bins for dsDNA - polyCG (a) and dsRNA - CG (b). Green lines represent the normalized populations of the slide bins. The regions of the h-rise against λ representation where the population was very small have been truncated due to the larger error, although they were taken into account for the estimation of $\lambda(f)$ by means of Eq. S23.

S4.5 Variation of the slide upon stretching

The discussion in Section S4.4 and in the main text (Fig. 2a) ascribes the increase or decrease of the stretch modulus to the change in the slide upon pulling. The different slide variation of dsDNA and dsRNA was noticed in precedent studies.[5] In this section, we further inspect the sequences displaying the most extreme behaviors with respect to the variation of the slide: PolyCG of dsDNA with $\Delta\lambda/|\lambda(f = 1pN)| \approx 19.9\%$, and CG of dsRNA with $\Delta\lambda/|\lambda(f = 1pN)| \approx -8.5\%$, for which we compute the h-rise and slide of every step of the trajectory at $f = 1\ pN$.

Fig. S8 displays the correlation between slide and h-rise (h) for dsDNA - PolyCG Fig.S8a and dsRNA - CG Fig.S8b. In this regard, we divided the range of observed values of λ in bins of size equal to 0.04 nm and, for each bin, we computed the average h-rise of the corresponding simulation frames. Green lines display the populations of each slide bin, which were shifted by an arbitrary constant to enable simultaneous plotting of the populations and the correlations. We see how the majority of frames lies within the $h'(\lambda) > 0$ region for dsDNA ($\approx 69\%$ of the population) and within the $h'(\lambda) < 0$ region for dsRNA ($\approx$ 71 % of the population). The stretching force exerts a work $-f\Delta h$ per step, so that larger values of h are more favorable. This notion explains why $|\lambda| \to 0$ for dsDNA, given the fact that dsDNA steps have the property $h'(\lambda) > 0$ with $\lambda < 0$ (Fig. S8 (a)), while $|\lambda| \to \infty$ for dsRNA, provided that in this case $h'(\lambda) < 0$ with $\lambda < 0$ (Fig. S8 (b)).

Furthermore, the $\{\lambda, h\}$ graphs in Fig. S8 may be taken as a map $h : \{\lambda\} \to \{h - rise\}$, and used to estimate the expected evolution of the slide with the stretching force via free-energy perturbation.[8] We write the potential energy of the Hamiltonian of our system as

$$U(\bar{\boldsymbol{q}}, f) = U_0(\bar{\boldsymbol{q}}) - fNh(\bar{\boldsymbol{q}})$$

being $\bar{\boldsymbol{q}}$ the set of atomic coordinates, $U_0(\vec{q})$ the potential energy in the absence of a force, N the number of steps, and $h(\vec{q})$ the h-rise. We then compute the average

$$\langle\lambda\rangle_f = \frac{\int \lambda(\bar{\boldsymbol{q}}) \exp[-\beta U_0(\bar{\boldsymbol{q}}) + \beta f N h(\bar{\boldsymbol{q}})] d\bar{\boldsymbol{q}}}{\int \exp[-\beta U_0(\bar{\boldsymbol{q}}) + \beta f N h(\bar{\boldsymbol{q}})] d\bar{\boldsymbol{q}}}$$

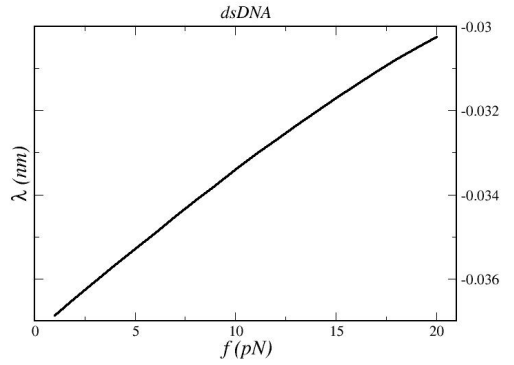

(a)

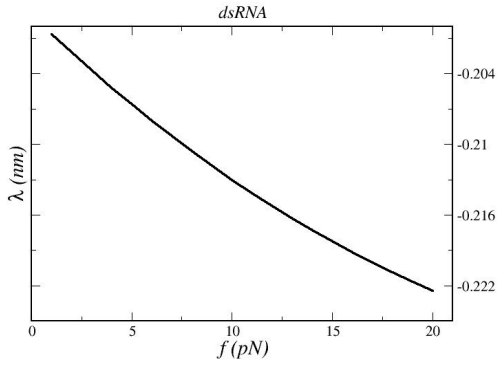

(b)

Figure S9: Prediction of evolution of slide upon stretching for dsDNA - polyCG (a) and dsRNA - CG (b).

being β the inverse of the thermal energy. Then we multiply and divide by $\int \exp[-\beta U_0(\bar{\boldsymbol{q}})]d\Gamma$, and rearrange to achieve

$$\langle\lambda\rangle(f) = \frac{\int \lambda(\bar{\boldsymbol{q}}) \exp[-\beta U_0(\bar{\boldsymbol{q}})] \exp[\beta f N h(\bar{\boldsymbol{q}})] d\Gamma}{\int \exp[-\beta U_0(\bar{\boldsymbol{q}})] d\Gamma} \times \left[\frac{\int \exp[-\beta U_0(\bar{\boldsymbol{q}})] \exp[\beta f N h(\bar{\boldsymbol{q}})] d\Gamma}{\int \exp[-\beta U_0(\bar{\boldsymbol{q}})] d\Gamma}\right]^{-1}$$

Which finally leads to

$$\langle\lambda\rangle_f = \frac{\langle\lambda \exp[\beta f N h]\rangle_{f=0}}{\langle\exp[\beta f N h]\rangle_{f=0}} \tag{S23}$$

Based on Eq. S23, we can predict the evolution of the slide with the stretching force (Fig. S9).

The prediction based on the free-energy perturbation provides a good estimation of the relative slide variation of the two molecules - $\Delta\lambda/|\lambda(f = 1pN)| \approx -21\%$ for dsDNA polyCG and $\Delta\lambda/|\lambda(f = 1pN)| \approx -10\%$ for dsRNA CG, to be compared with their respective values 19.9% and -8.5% obtained from the simulations at a pulling force of $20\,pN$. The estimation predicts a behavior of $\lambda(f)$ in good agreement with the simulations, thus providing a clear insight on the variation of the slide upon stretching, and ultimately on the variation of the stretch modulus.

S4.6 Variation of the twist-stretch coupling

Fig. S10 represents the $g'(f)$ resulting from the analysis of the fluctuations of the dsDNA and dsRNA sequences. As discussed in the main text, $g'(f) > 0$ for both molecules implies on one hand that the positive twist-stretch correlation of dsDNA vanishes, and that the negative twist-stretch correlation of dsRNA is enhanced on the other hand. The case of dsDNA, not only does have experimental support, but it can be also interpreted in terms of a force-mediated transition between two states of the steps.[5]

The results for dsRNA imply that the negative twist-stretch correlation increases upon pulling. In the next section, we demonstrate that a standard helical object with fixed radius would display $g'(f) < 0$ on top of $g(f) > 0$, which illustrates the non-triviality of the results displayed in Fig. S10.

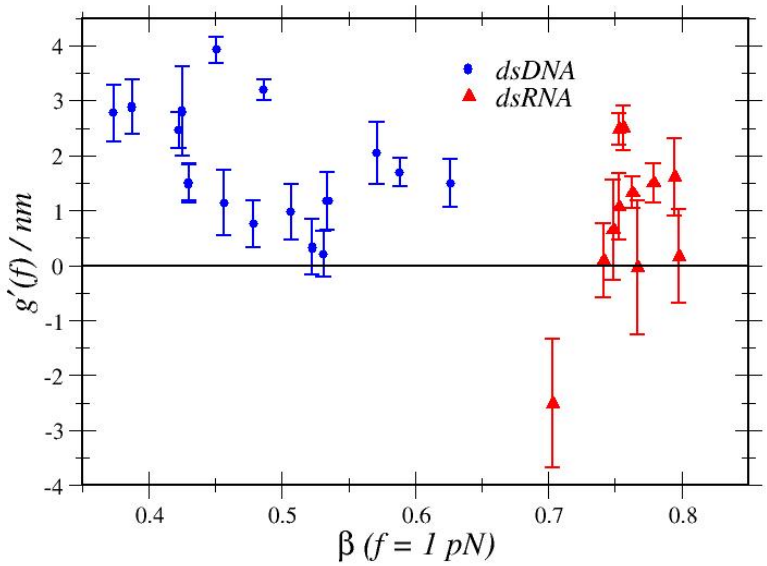

Figure S10: Variation of the twist stretch coupling with the stretching force for dsDNA (blue circles) and dsRNA (red triangles).

S4.7 Stretching a helix with fixed radius and fixed contour length

In this section, we compute $g(f)$ and $g'(f)$ for a helical object with fixed radius. The helical frequency, ω, is the parameter that matches best the concept of *twist*. A helix with smaller pitch P will have a larger number of turns per unit height than another helix of the same radius with larger P, which translates into a larger ω and would be interpreted ultimately as having a larger twist. From Eq. S16 and the fact that $h = \frac{2\pi}{N\omega}$ it is possible to write

$$\omega(L) = \frac{2\pi}{N}\sqrt{\left[L^2 - \left(\frac{2\pi r}{N}\right)^2\right]^{-1}} \tag{S24}$$

and then expand $\omega(h + \Delta h)$ for small deformations, i. e. $\Delta h \ll 1$, to achieve

$$\omega(h + \Delta h) = \omega_0 + \omega_1 \Delta h + \omega_2 \Delta h^2 + \mathcal{O}(\Delta h^3) \tag{S25}$$

$$\omega_0 = \omega(h)$$

$$\omega_1 = -\frac{2\pi L}{N}\left[L^2 - \left(\frac{2\pi r}{N}\right)^2\right]^{-3/2}$$

$$\omega_2 = \frac{2\pi}{N}\frac{L^2N^2 + 2\pi^2 r^2}{\left[L^2 - \left(\frac{2\pi r}{N}\right)^2\right]^2}\sqrt{\left[L^2 - \left(\frac{2\pi r}{N}\right)^2\right]^{-1}}$$

Since $\omega \in \mathbb{R}^+$, it must be $L > \frac{2\pi r}{N}$, so that independently of the particular values of the parameters, $\omega_1 < 0$ and $\omega_2 > 0$. The former implies $g(f) > 0$ for a helical object of constant radius, i. e. that stretching and twisting are negatively correlated. The latter, on the other hand, implies that $g'(f) < 0$, meaning that such negative correlation is being cut down upon pulling. Interestingly, $\lim_{L\to\infty}(\omega_1) = \lim_{L\to\infty}(\omega_2) = 0$, which means that at some point $g(f) = 0$ and the correlation is completely lost. This observation highlights the fact that our findings for dsRNA are far from trivial.

As a final word, all along this derivation we have assumed that r is constant and independent of the stretching force. In order to make this problem mathematically solvable right away, some assumption of this kind must be made. On the other hand, the negative twist-stretch coupling of dsDNA has been connected in previous studies[7] to the radius of the helix being reduced upon pulling, so that it is clear that for dsDNA the assumption of a constant r does not hold.

References

[1] Gross, Peter, et al., *Quantifying how DNA stretches, melts and changes twist under tension*, Nature Physics, **7.9**, pp. 731-736 (2011).

[2] Marin-Gonzalez, Alberto, et al., *DNA crookedness regulates DNA mechanical properties at short length scales*, Physical Review Letters, **122**, pp. 048102 (2019).

[3] Assenza, Salvatore, and Pérez, Rubén, *Accurate Sequence-Dependent Coarse-Grained Model for Conformational and Elastic Properties of Double-Stranded DNA*, Journal of chemical theory and computation, **18.5**, pp. 3239-3256 (2022).

[4] Lipfert, Jan, et al., *Double-stranded RNA under force and torque: similarities to and striking differences from double-stranded DNA*, Proceedings of the National Academy of Sciences, **111.43**, pp. 15408-15413 (2014).

[5] Marin-Gonzalez, Alberto, et al., *Understanding the mechanical response of double-stranded DNA and RNA under constant stretching forces using all-atom molecular dynamics*, Proceedings of the National Academy of Sciences, **114.27**, pp. 7049-7054 (2017).

[6] Marin-Gonzalez, Alberto, et al., *Sequence-dependent mechanical properties of double-stranded RNA*, Nanoscale, **11.44**, pp. 21471-21478 (2017).

[7] Gore, Jeff, et al., *DNA overwinds when stretched*, Nature, **442.7104**, pp. 836-839 (2006).

[8] Frenkel, Daan and Smit, Berend, *Understanding molecular simulation: from algorithms to applications*, Elsevier (2001)

S5 Figures compilation

S5.1 A4GGA4 - Fig. S11

S5.2 A4TA4 - Fig. S12

S5.3 A8GG - Fig. S13

S5.4 A8T - Fig. S14

S5.5 DDD - Fig. S15

S5.6 DNAall - Fig. S16

S5.7 DUE - Fig. S17

S5.8 G4AAG4 - Fig. S18

S5.9 G4CG4 - Fig. S19

S5.10 polyA - Fig. S20

S5.11 polyAC - Fig. S21

S5.12 polyAG - Fig. S22

S5.13 polyAT - Fig. S23

S5.14 polyCG - Fig. S24

S5.15 polyG - Fig. S25

S5.16 TATA - Fig. S26

S5.17 TFBS - Fig. S27

S5.18 AA - Fig. S28

S5.19 AC - Fig. S29

S5.20 AG - Fig. S30

S5.21 AU - Fig. S31

S5.22 CG - Fig. S32

S5.23 GG - Fig. S33

S5.24 seq1 - Fig. S34

S5.25 seq2 - Fig. S35

S5.26 seq3 - Fig. S36

S5.27 seq4 - Fig. S37

S5.28 RNAall - Fig. S38

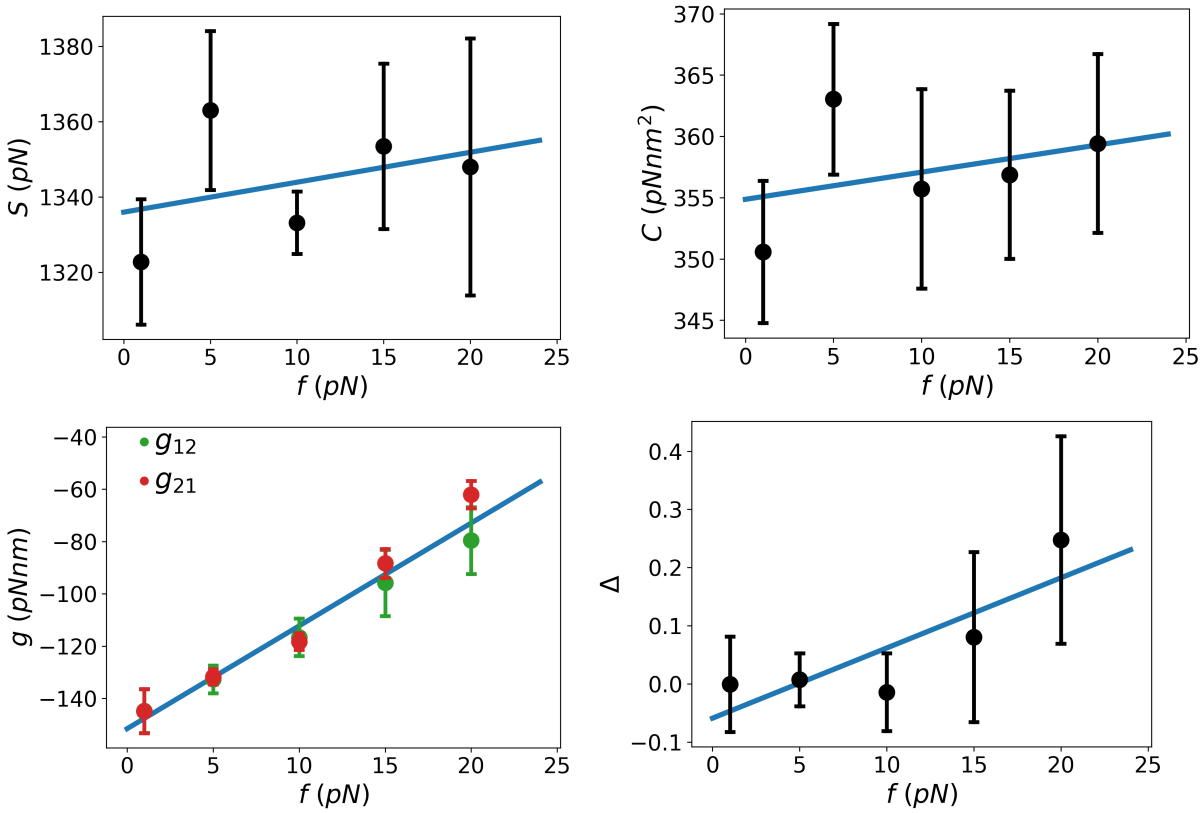

Figure S11: Force dependence of elastic parameters and constraint of A4GGA4.

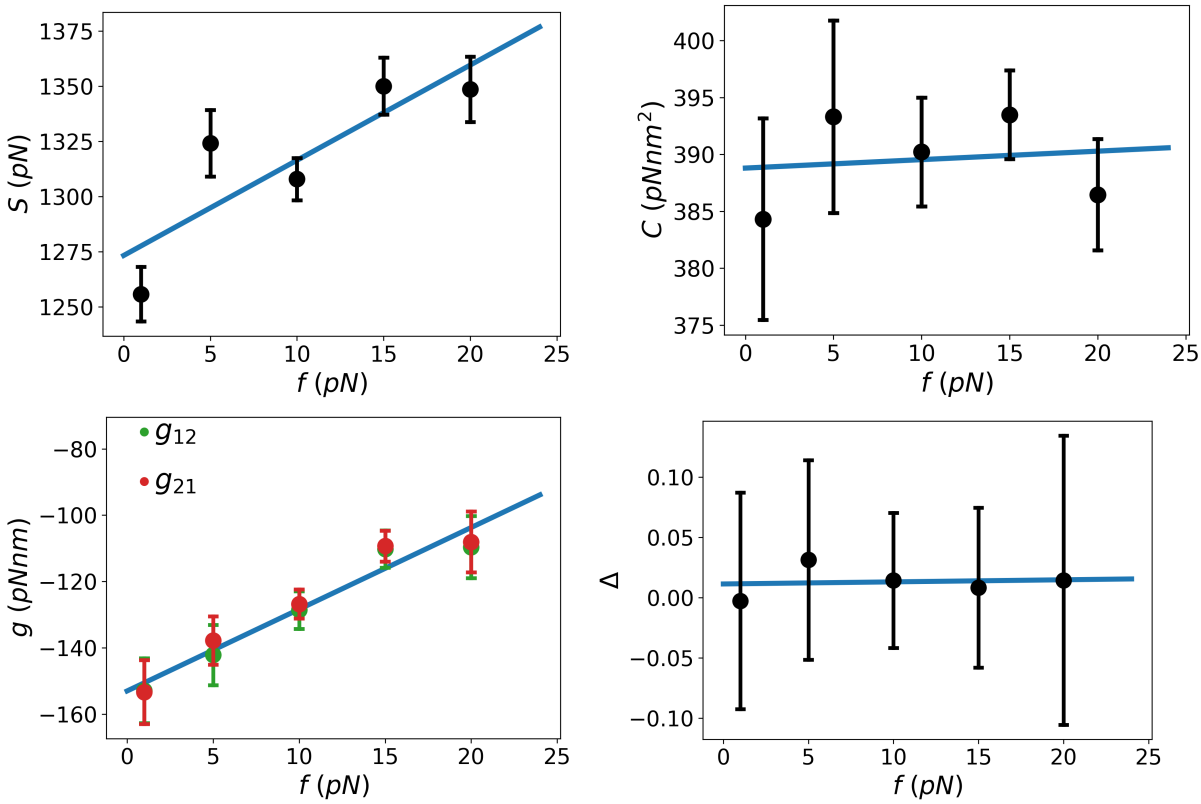

Figure S12: Force dependence of elastic parameters and constraint of A4TA4.

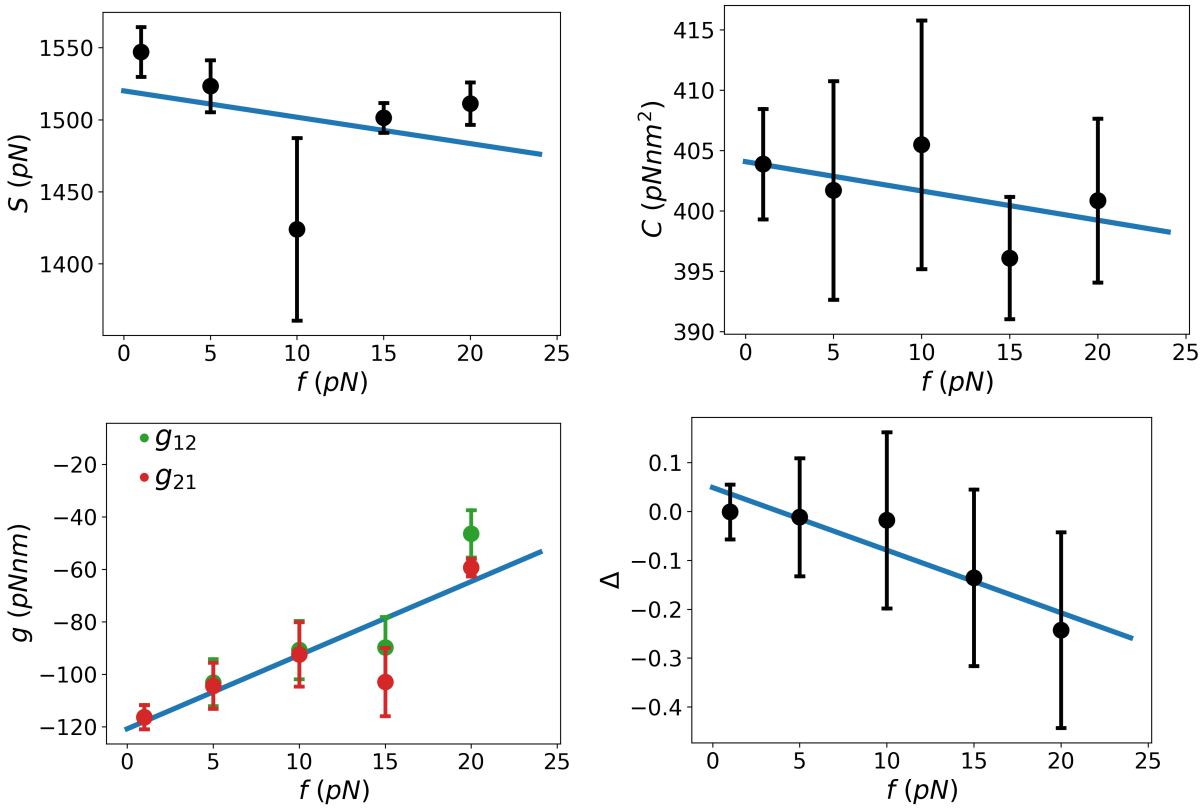

Figure S13: Force dependence of elastic parameters and constraint of A8GG.

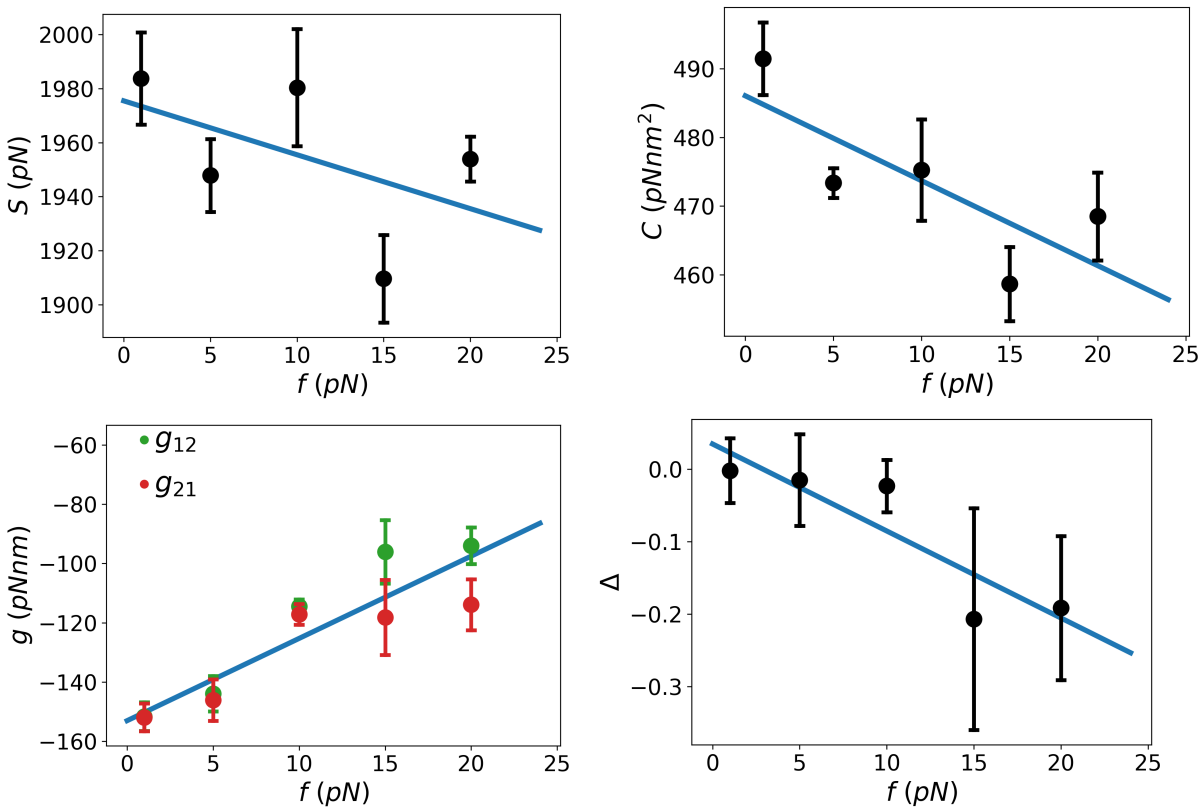

Figure S14: Force dependence of elastic parameters and constraint of A8T.

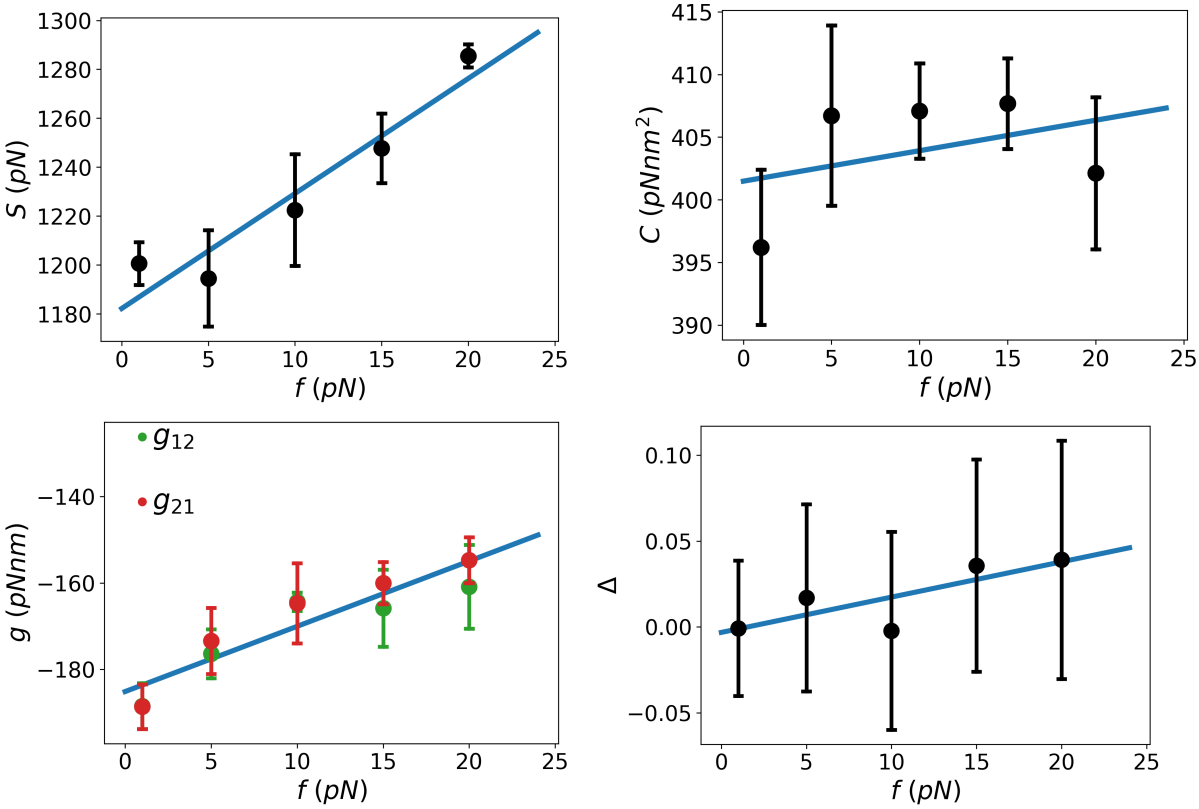

Figure S15: Force dependence of elastic parameters and constraint of DDD.

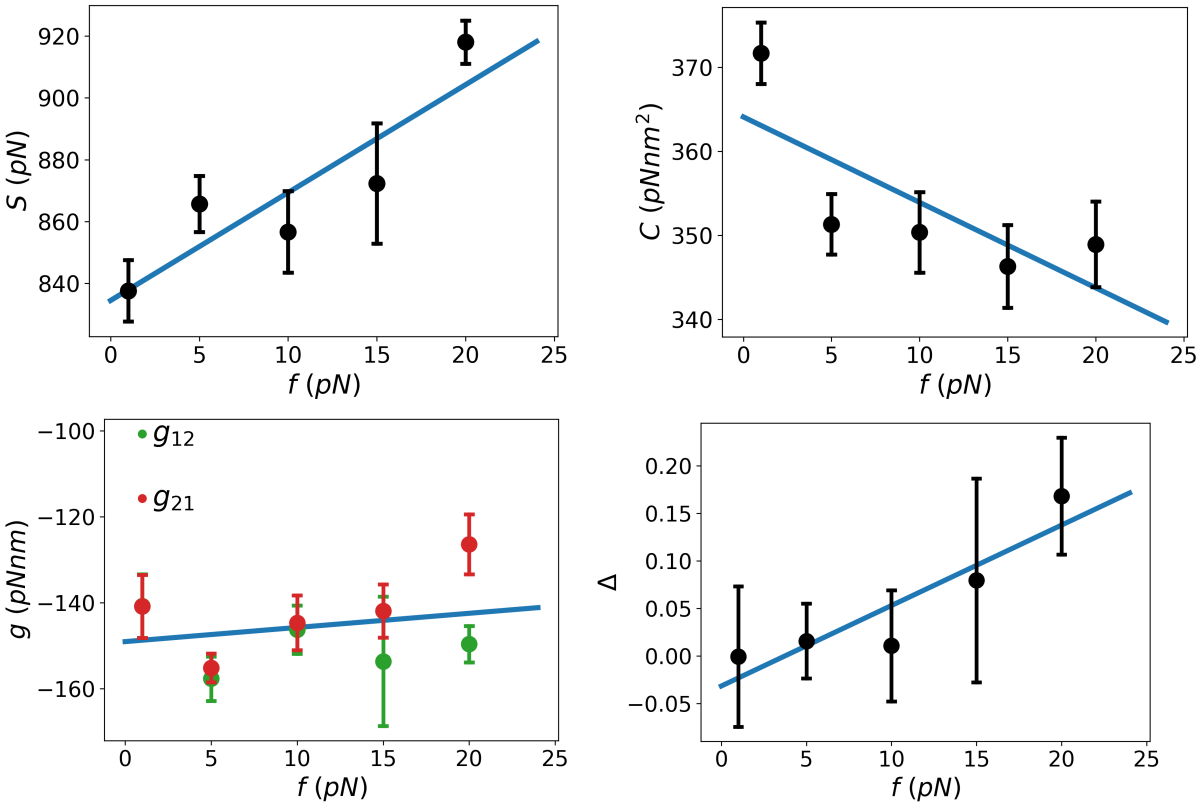

Figure S16: Force dependence of elastic parameters and constraint of DNAall.

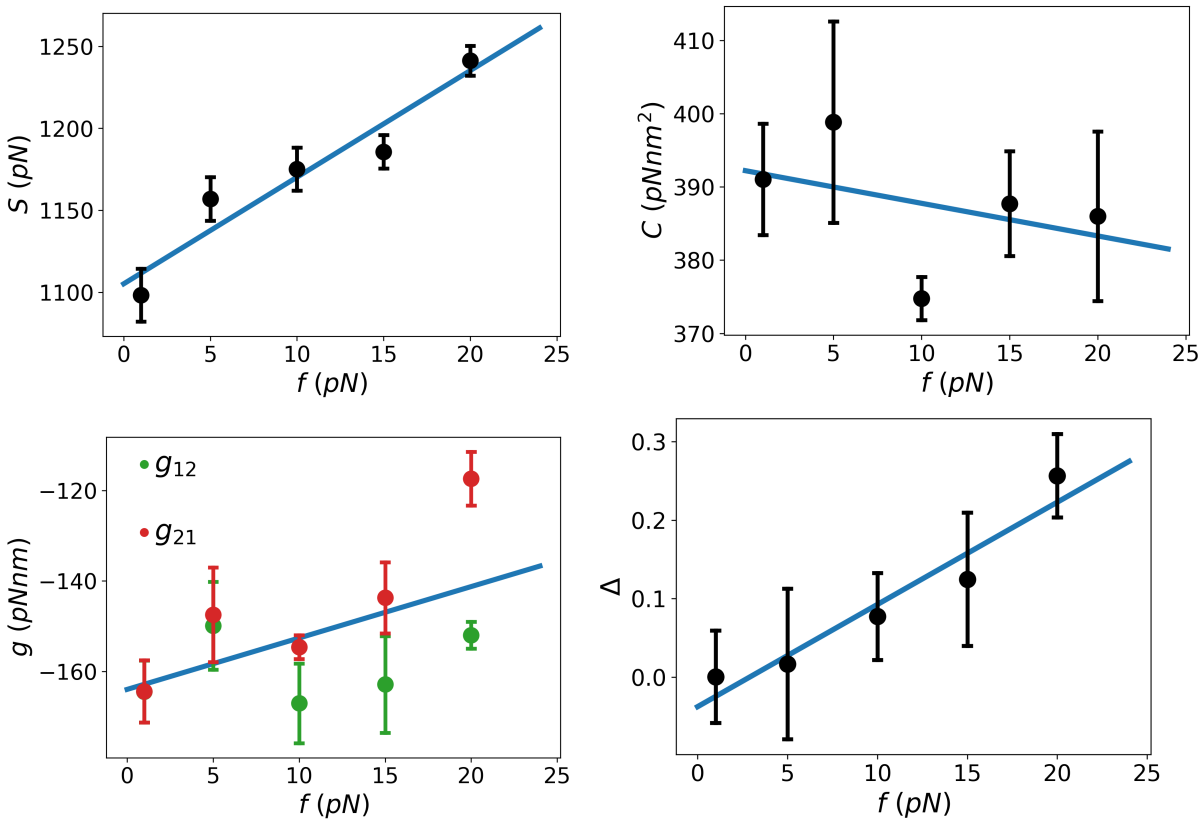

Figure S17: Force dependence of elastic parameters and constraint of DUE.

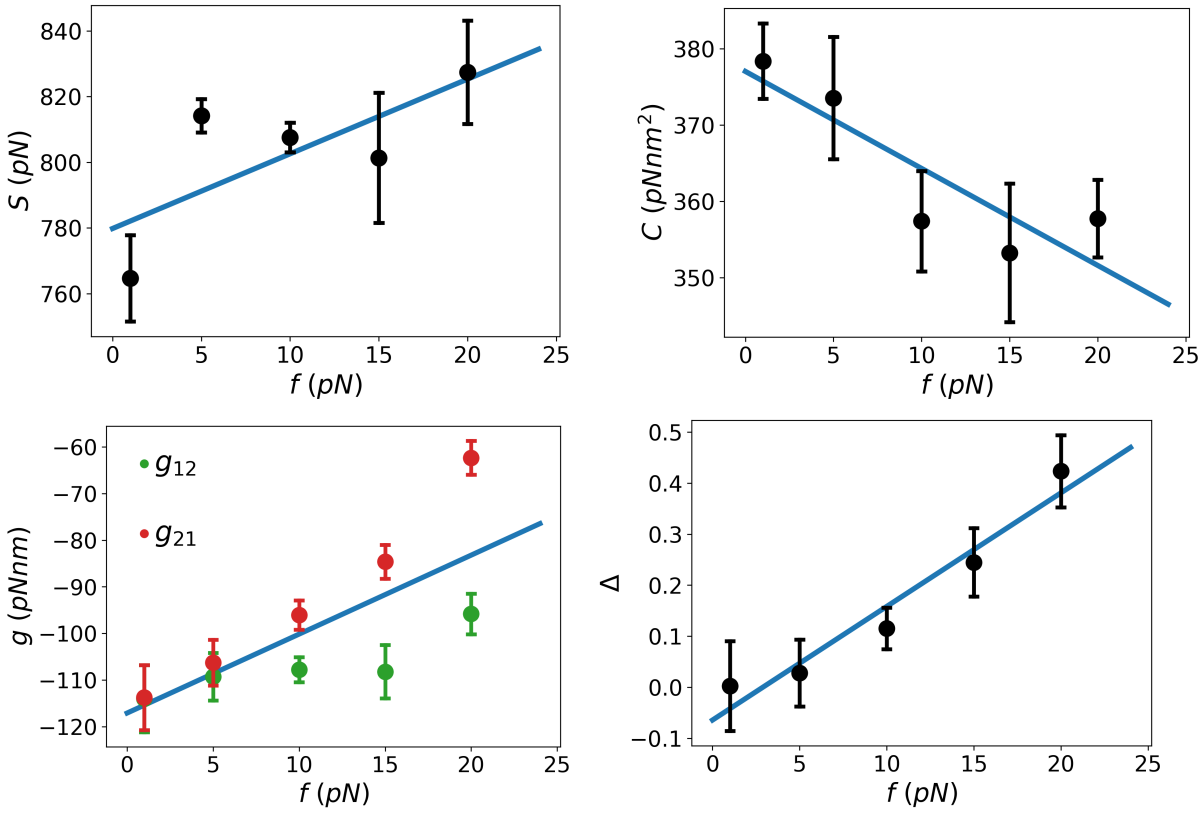

Figure S18: Force dependence of elastic parameters and constraint of G4AAG4.

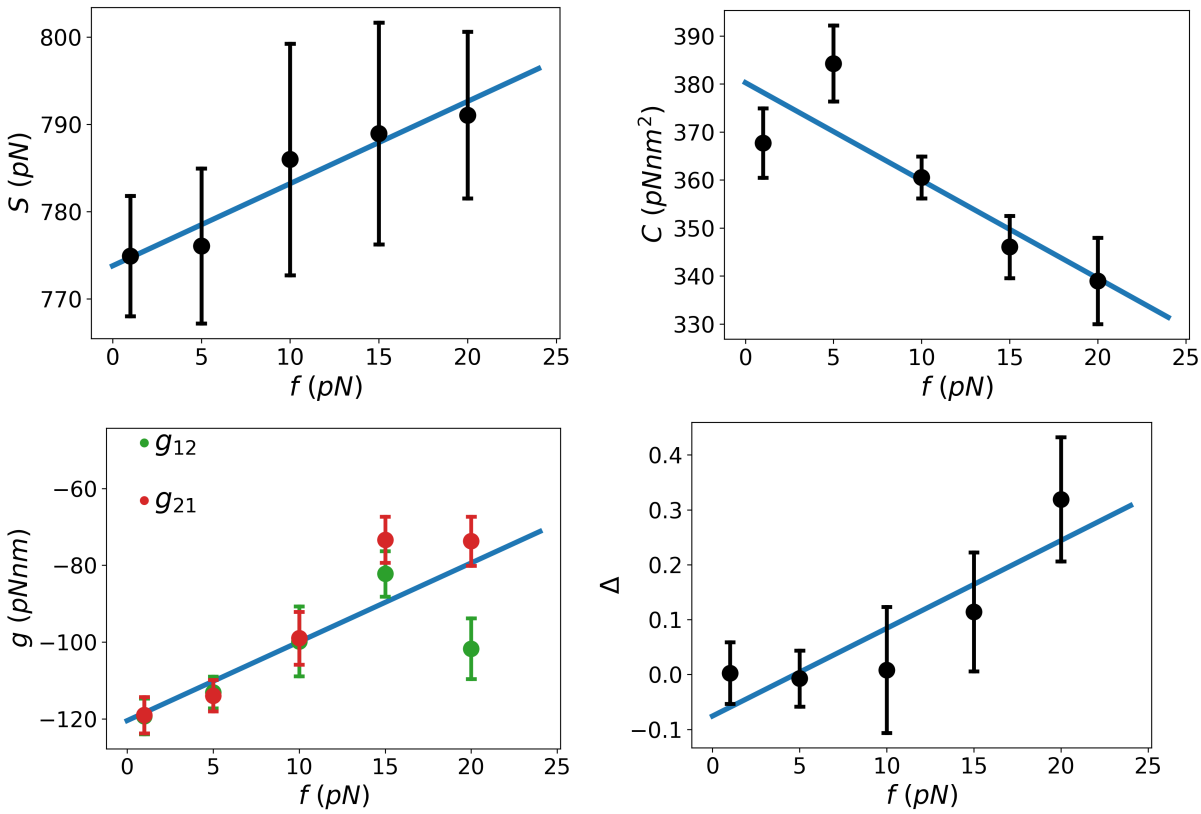

Figure S19: Force dependence of elastic parameters and constraint of G4CG4.

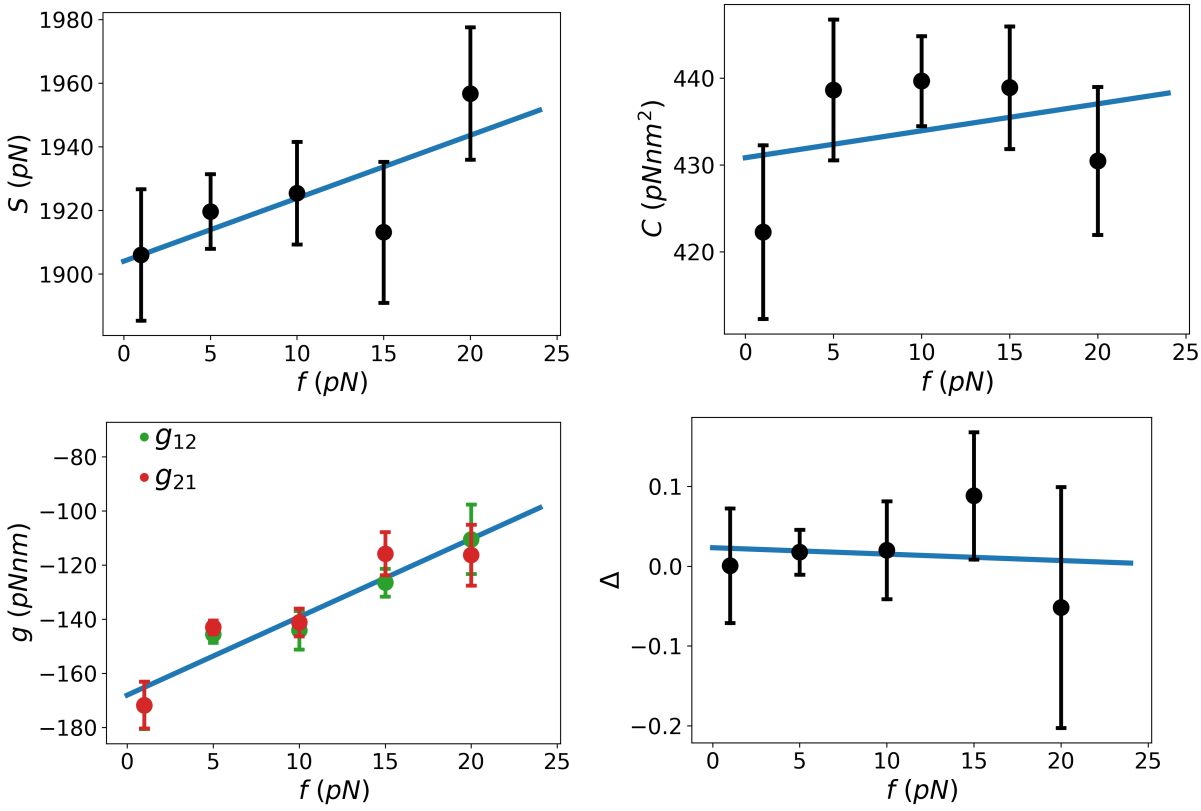

Figure S20: Force dependence of elastic parameters and constraint of polyA.

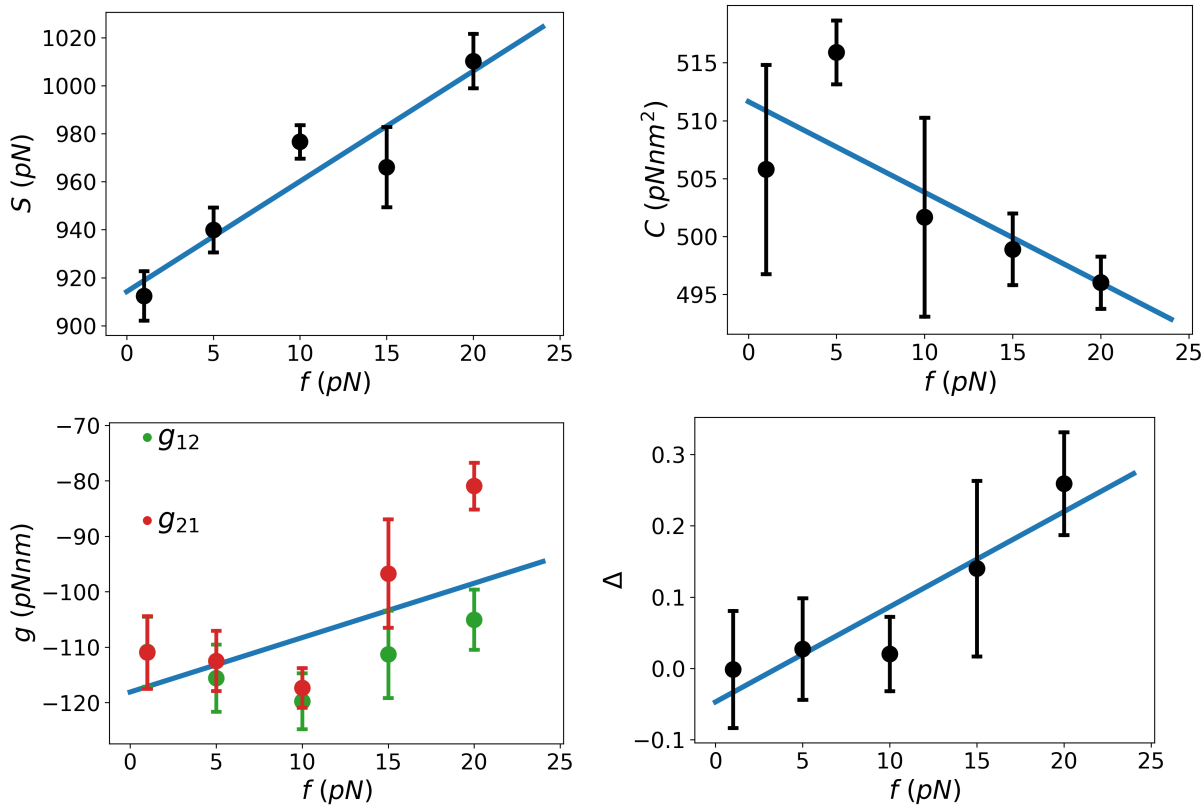

Figure S21: Force dependence of elastic parameters and constraint of polyAC.

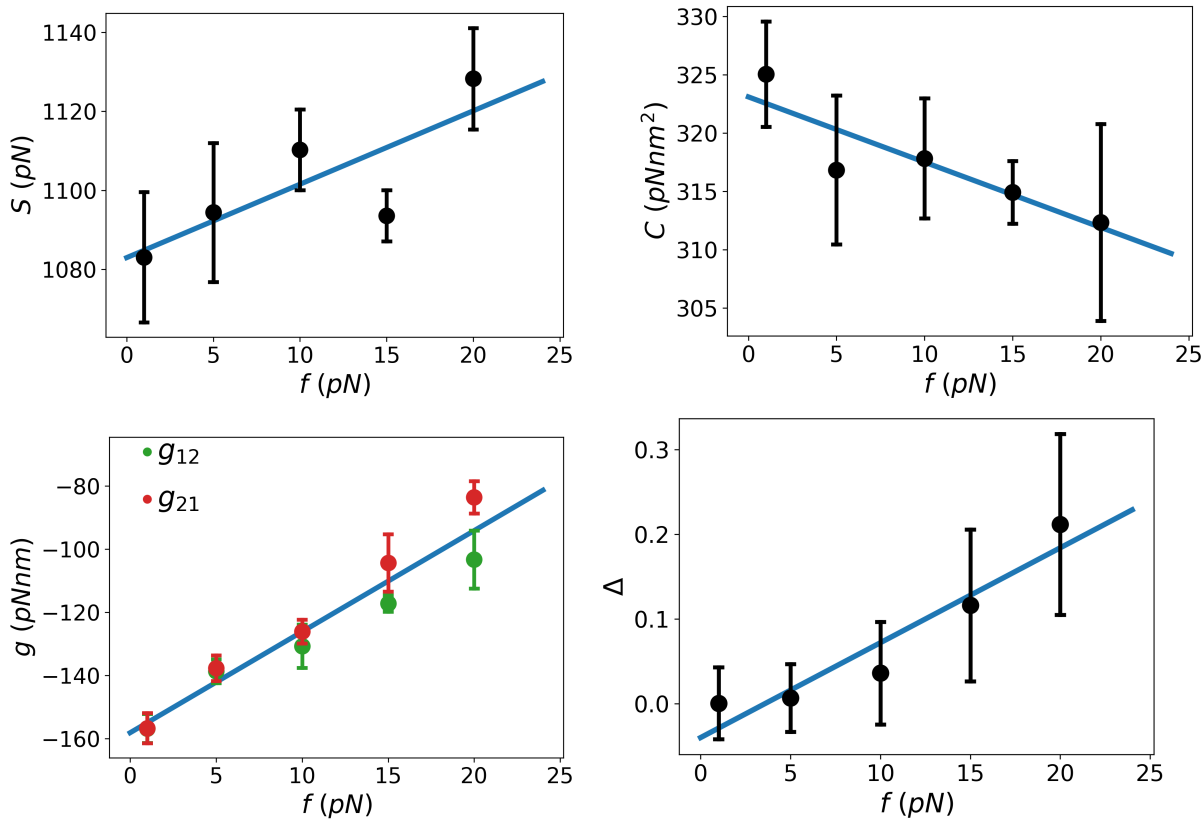

Figure S22: Force dependence of elastic parameters and constraint of polyAG.

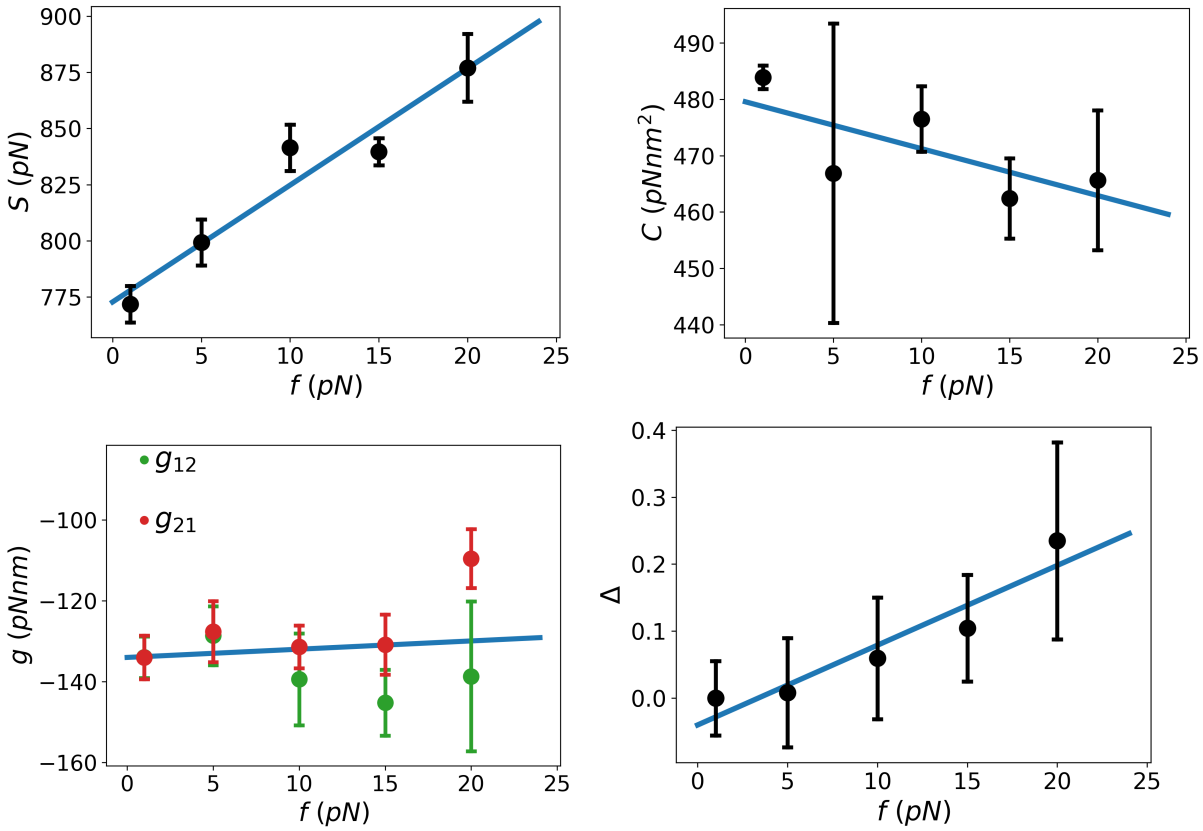

Figure S23: Force dependence of elastic parameters and constraint of polyAT.

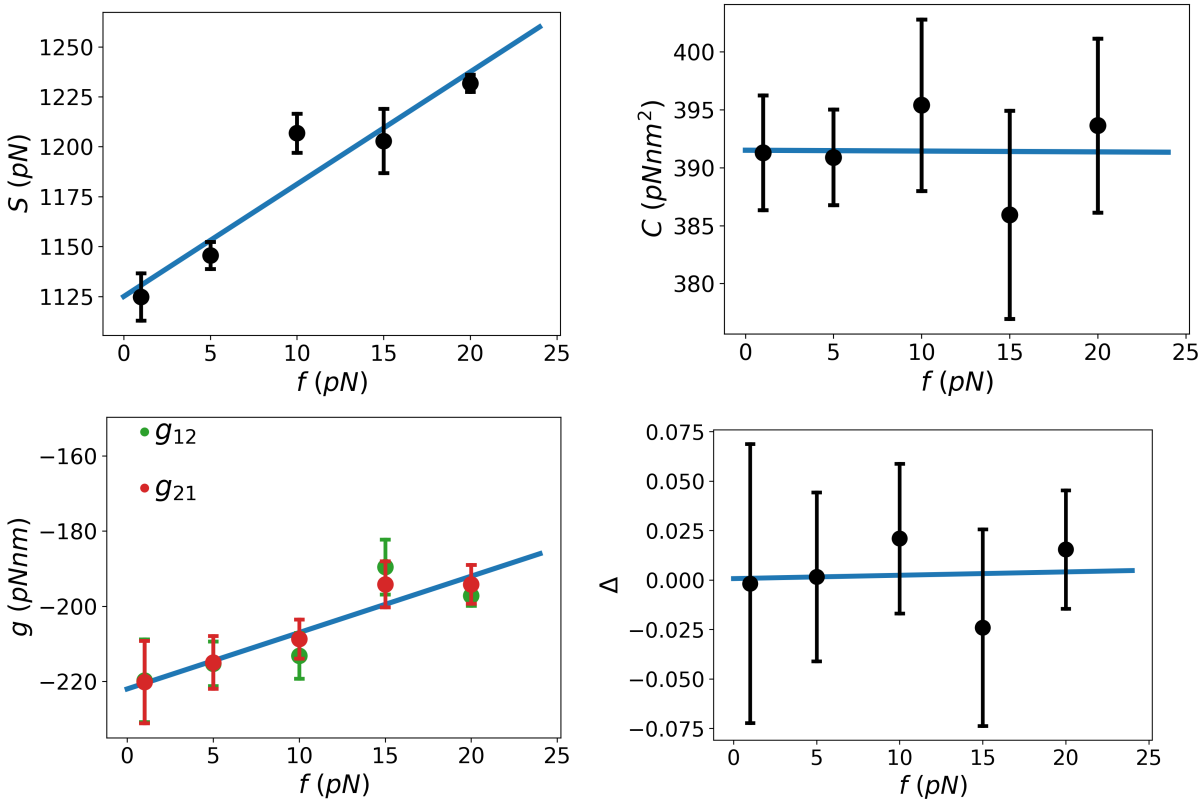

Figure S24: Force dependence of elastic parameters and constraint of polyCG.

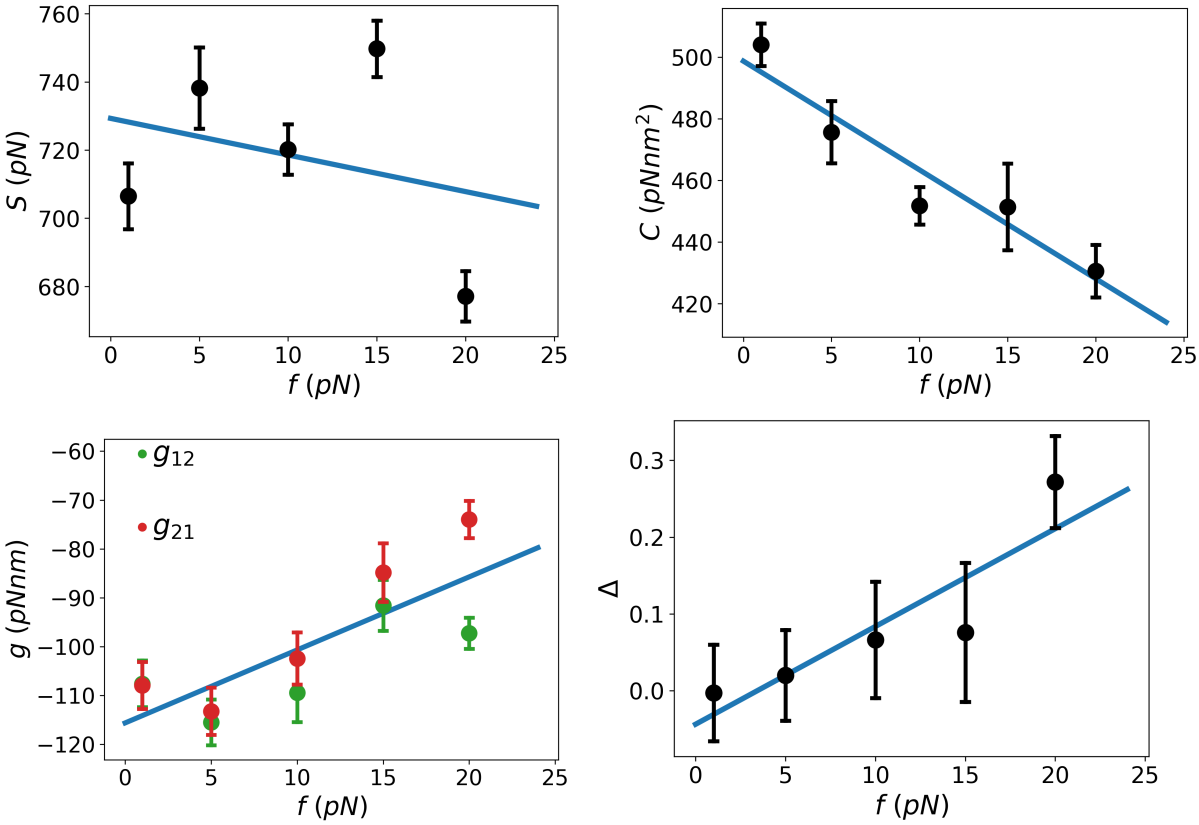

Figure S25: Force dependence of elastic parameters and constraint of polyG.

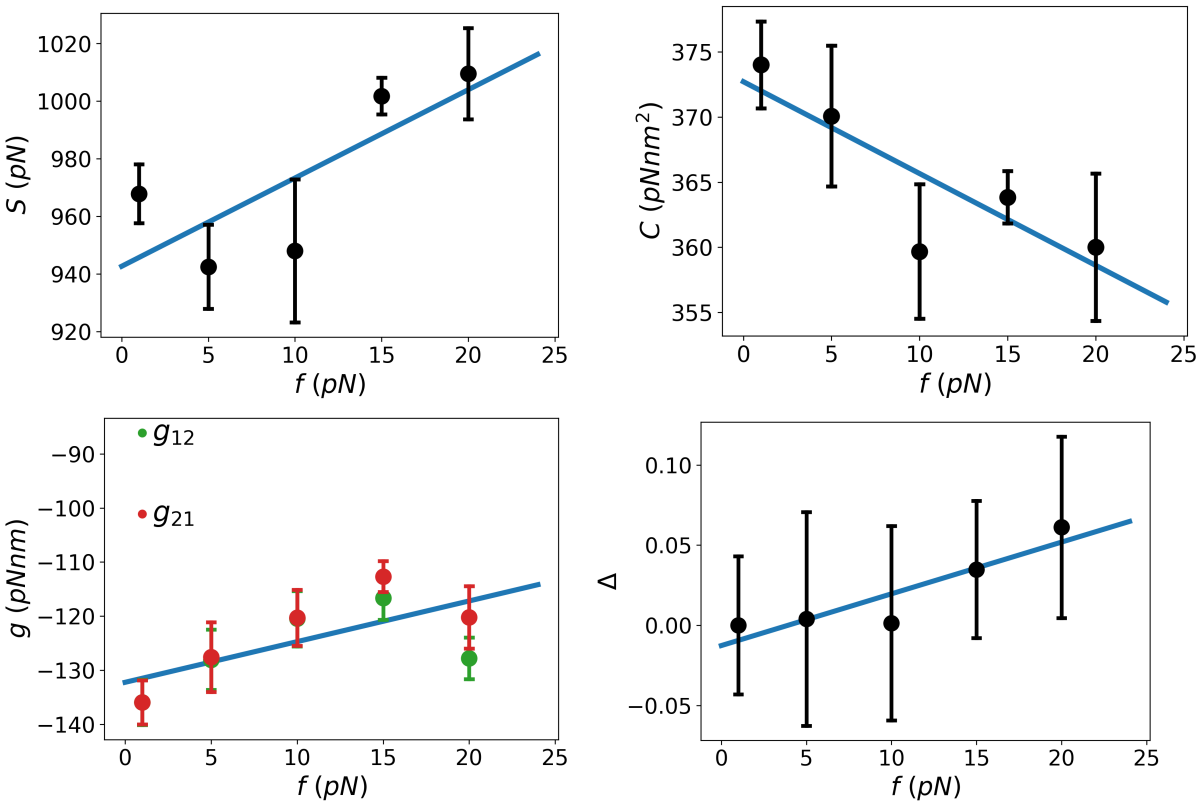

Figure S26: Force dependence of elastic parameters and constraint of TATA.

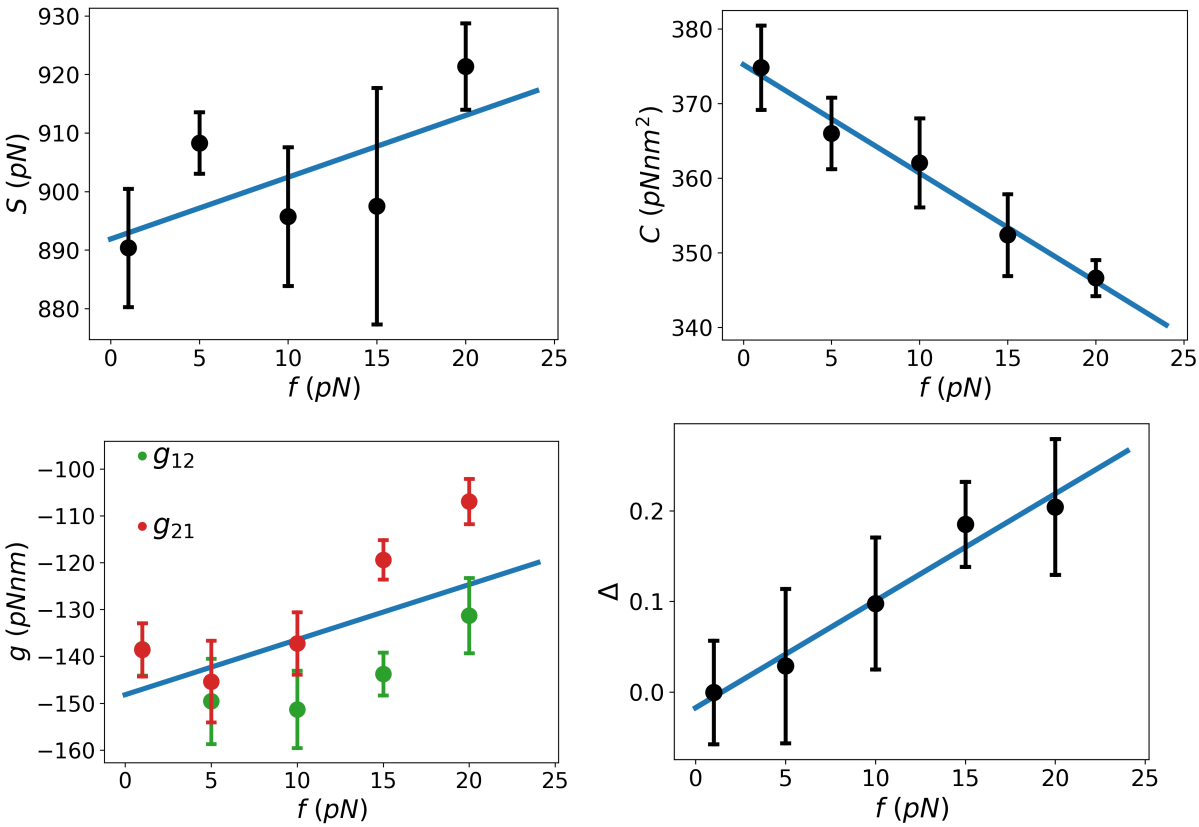

Figure S27: Force dependence of elastic parameters and constraint of TFBS.

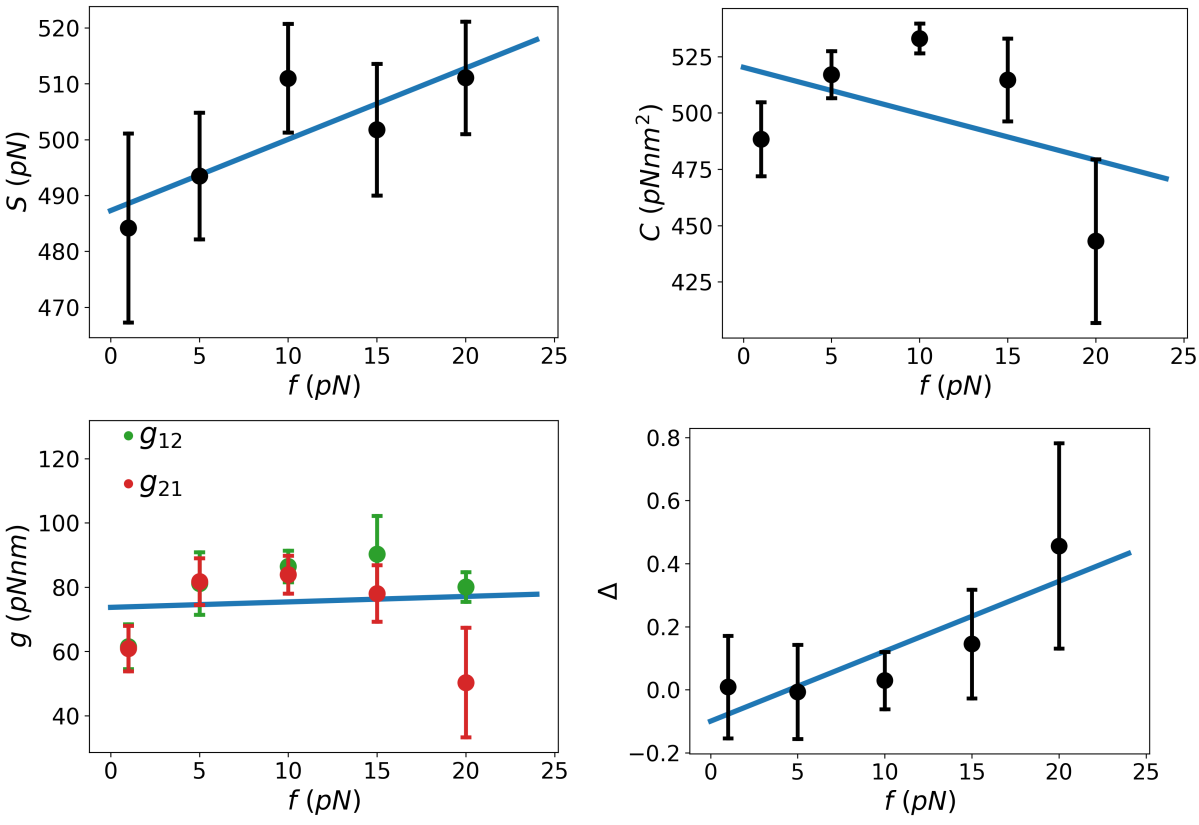

Figure S28: Force dependence of elastic parameters and constraint of AA.

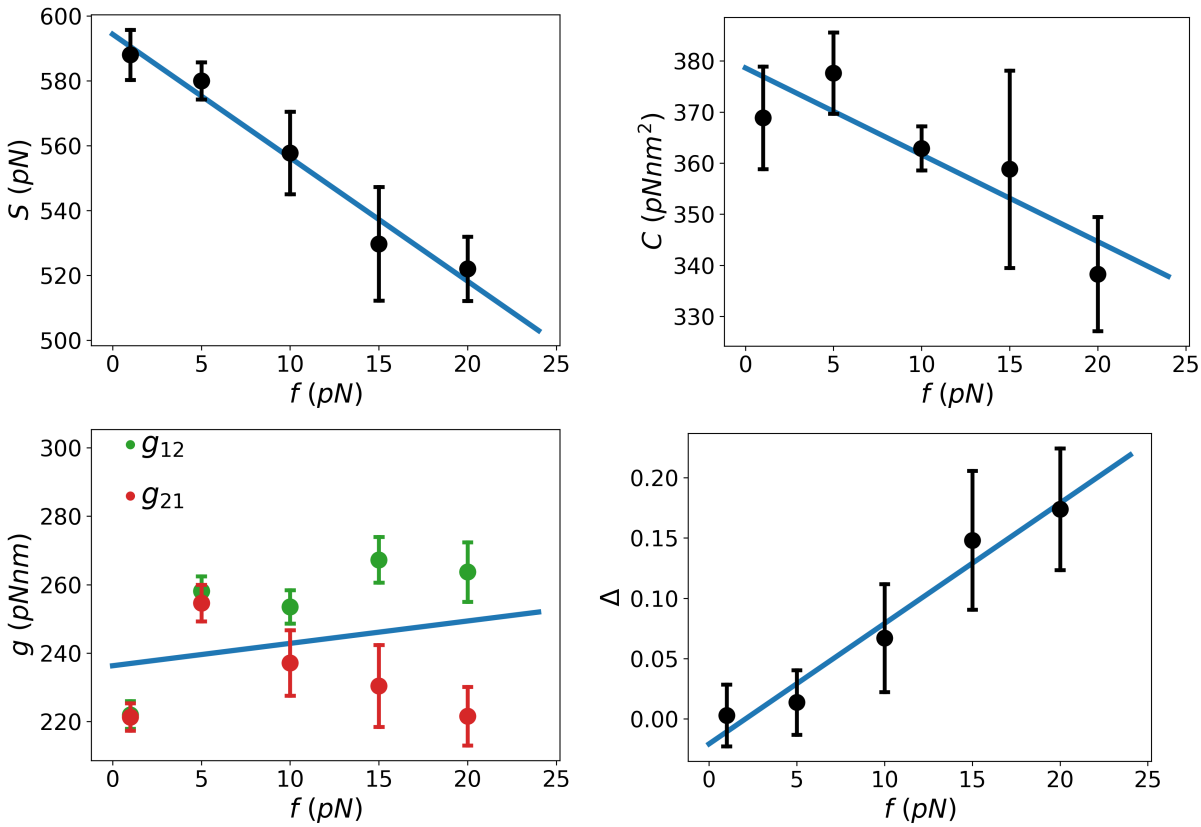

Figure S29: Force dependence of elastic parameters and constraint of AC.

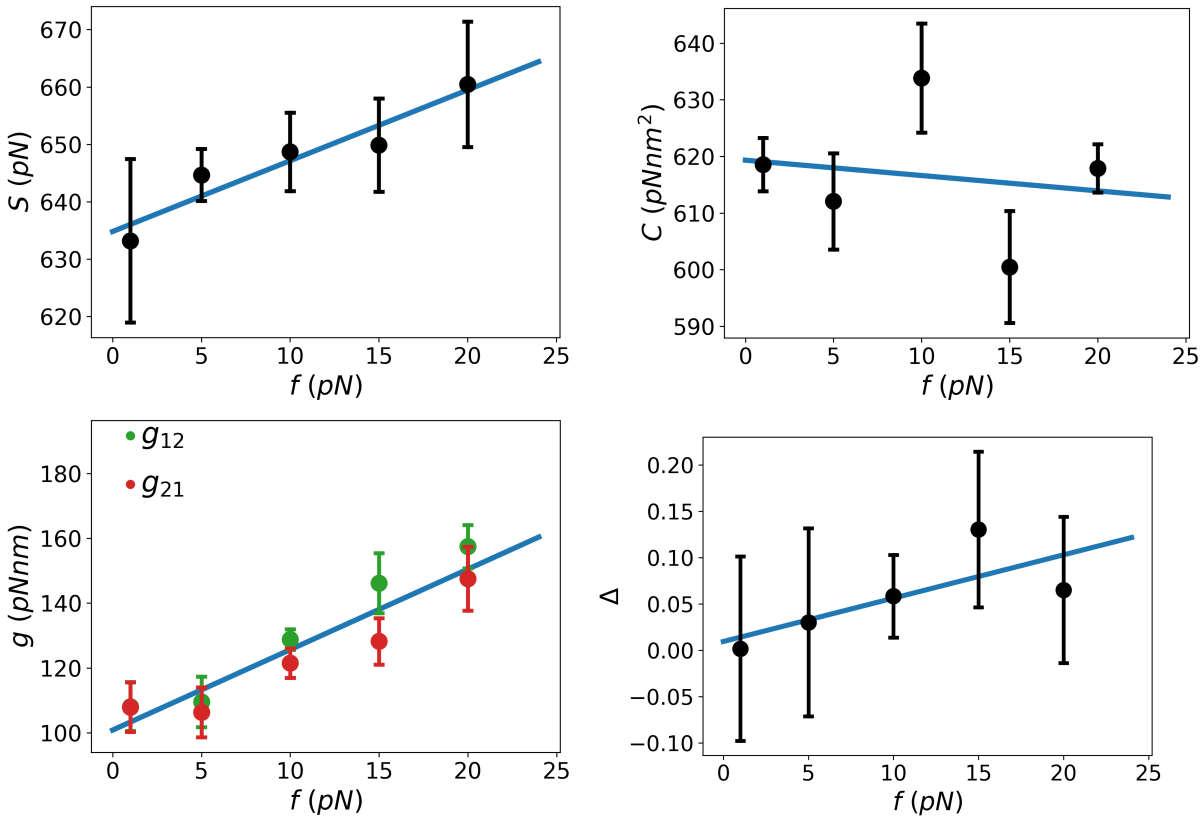

Figure S30: Force dependence of elastic parameters and constraint of AG.

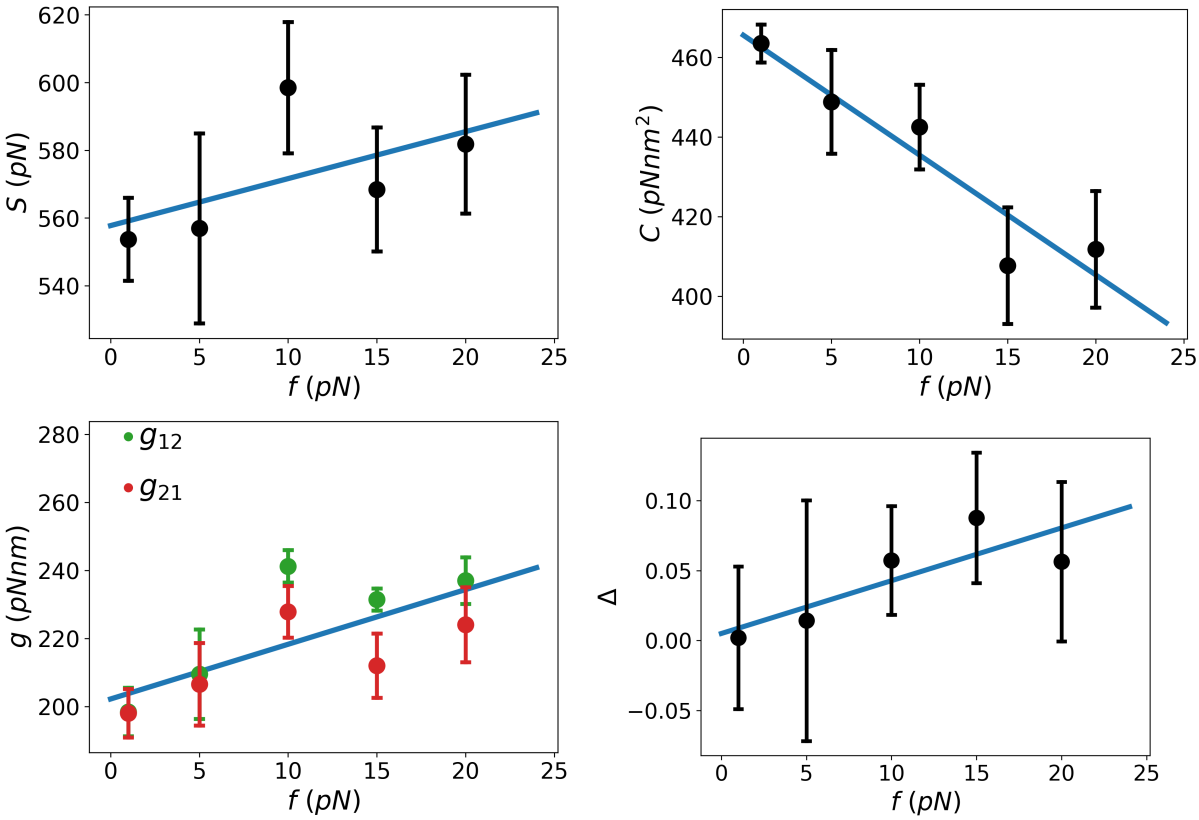

Figure S31: Force dependence of elastic parameters and constraint of AU.

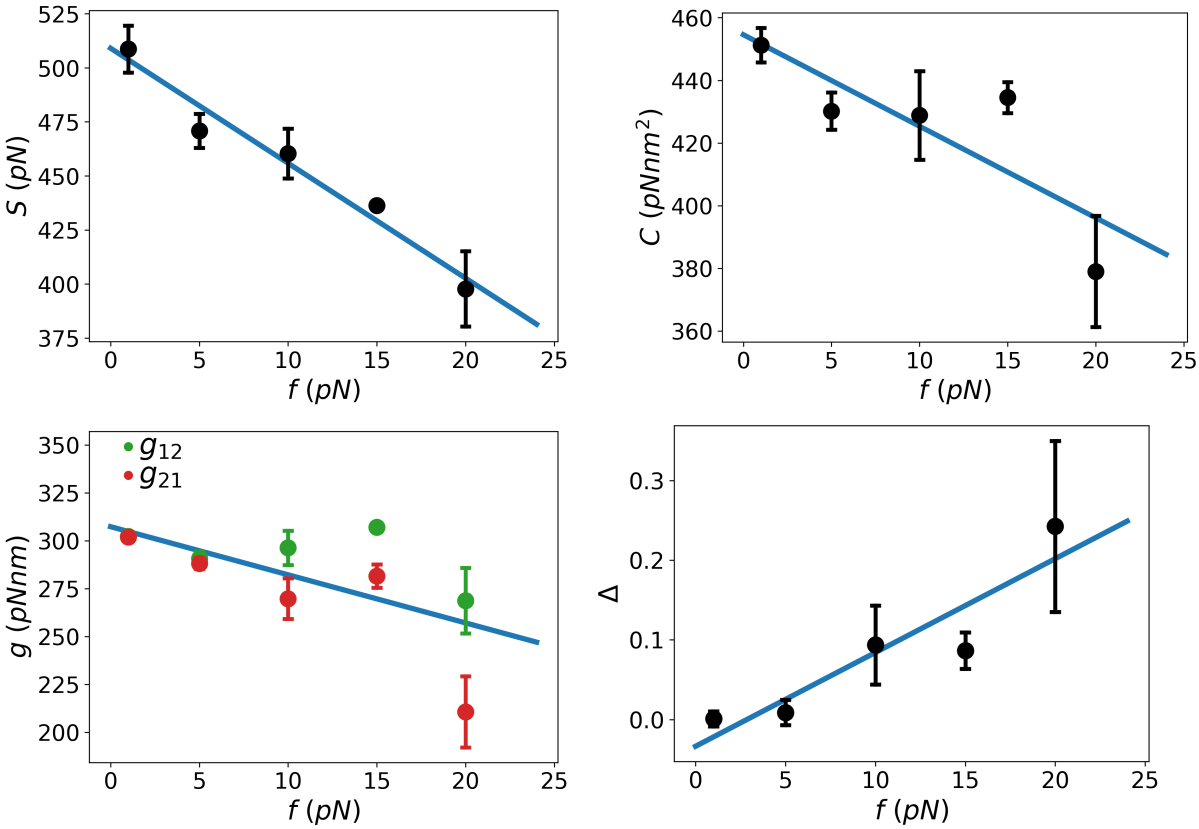

Figure S32: Force dependence of elastic parameters and constraint of CG.

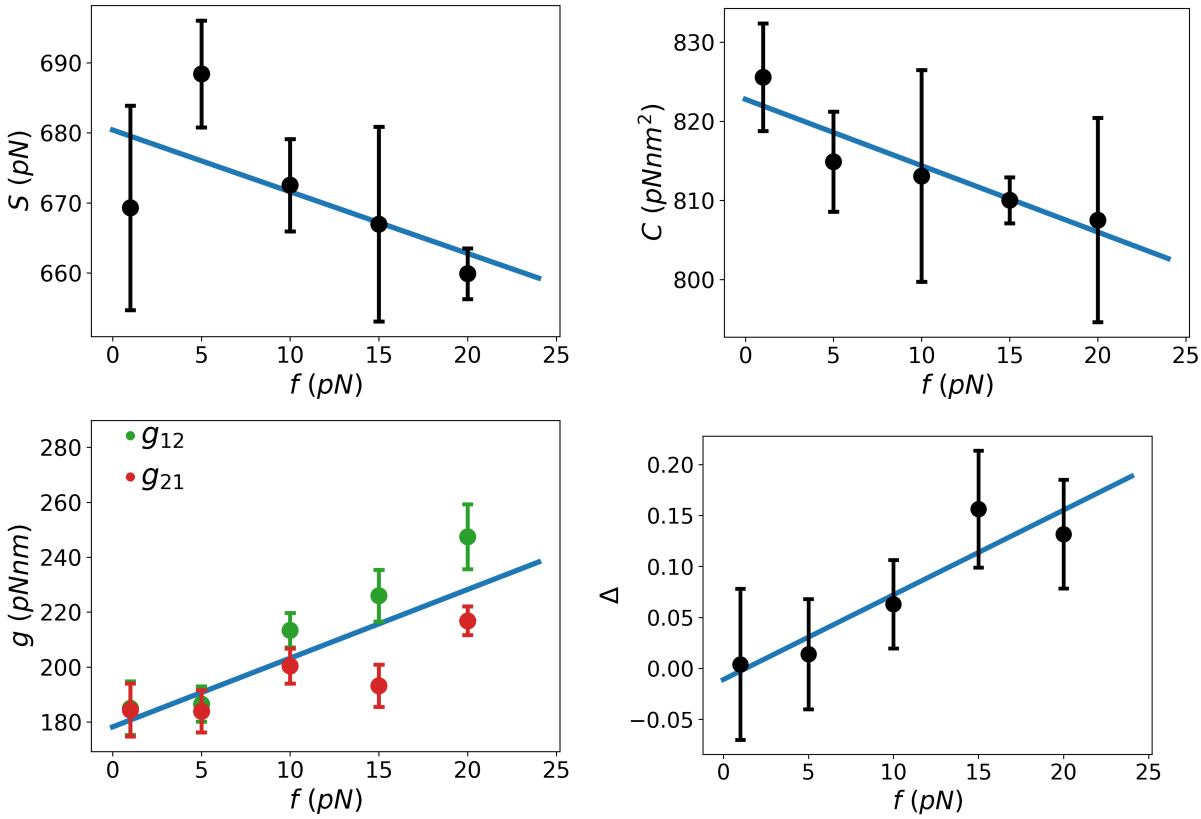

Figure S33: Force dependence of elastic parameters and constraint of GG.

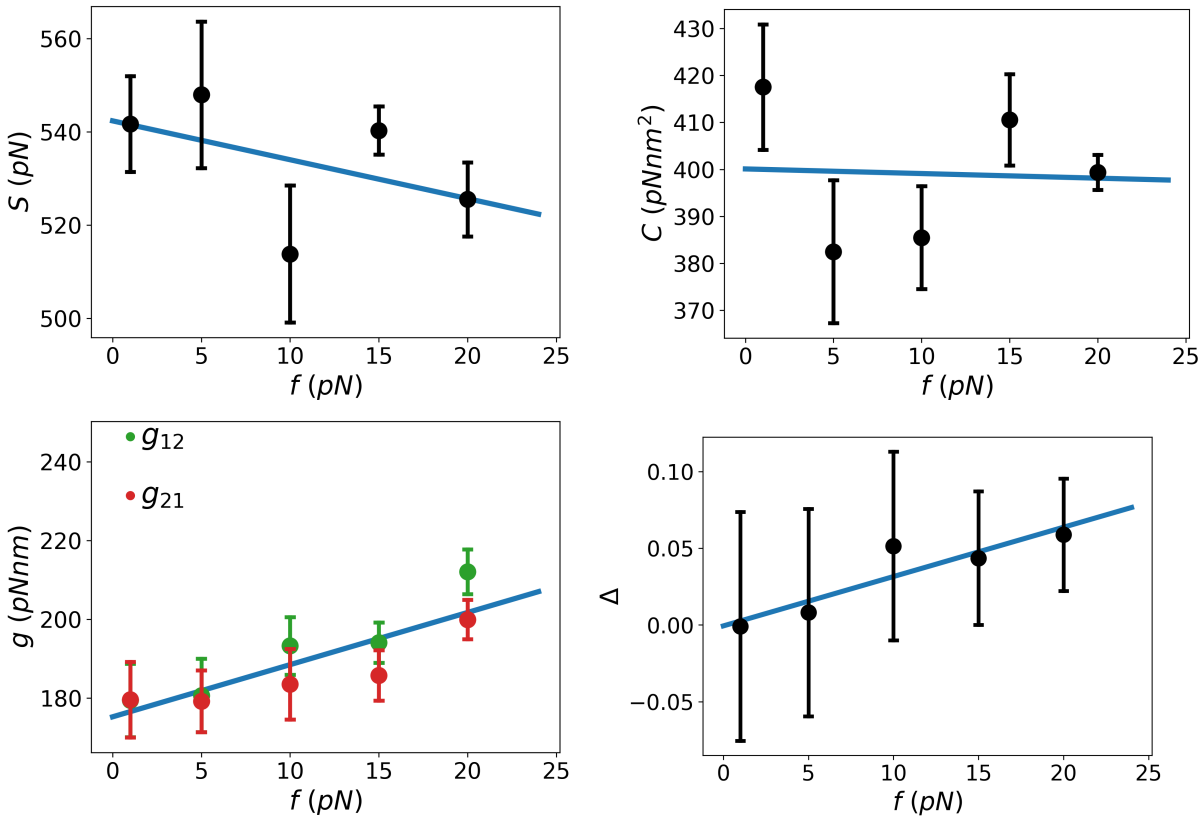

Figure S34: Force dependence of elastic parameters and constraint of seq1.

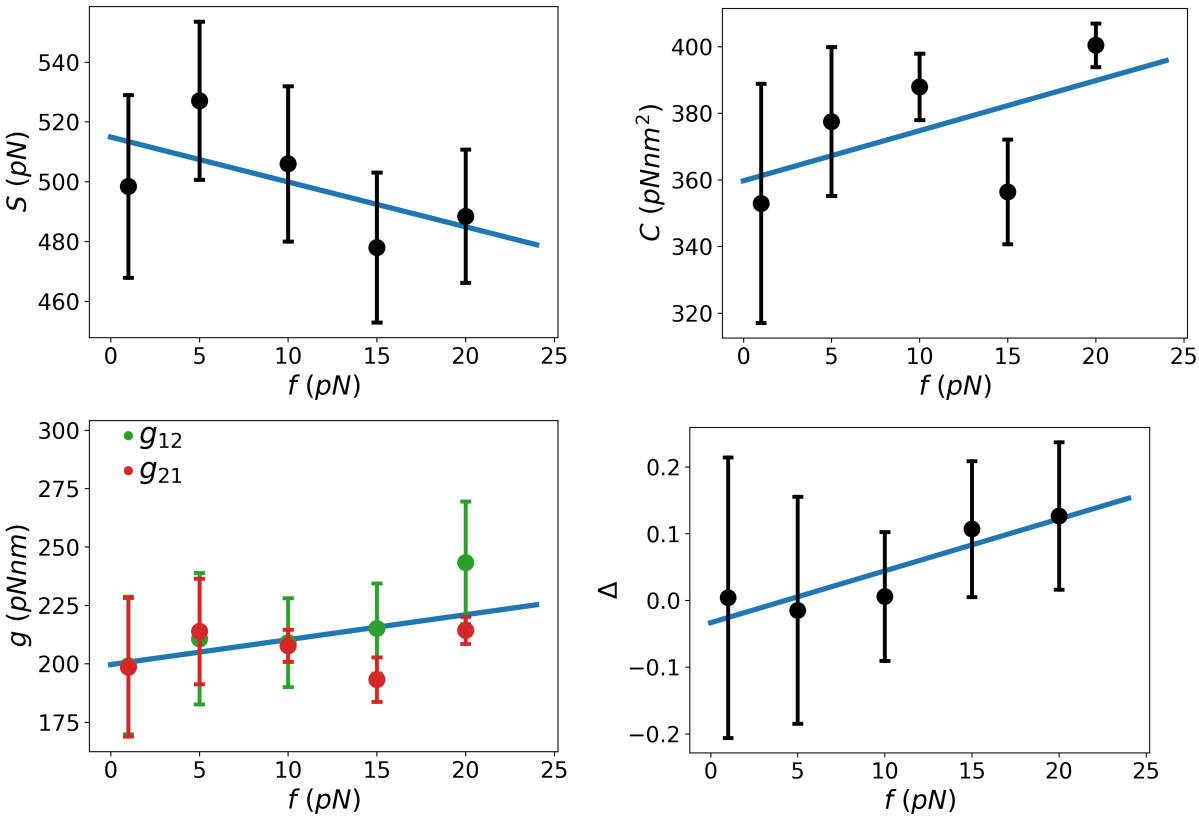

Figure S35: Force dependence of elastic parameters and constraint of seq2.

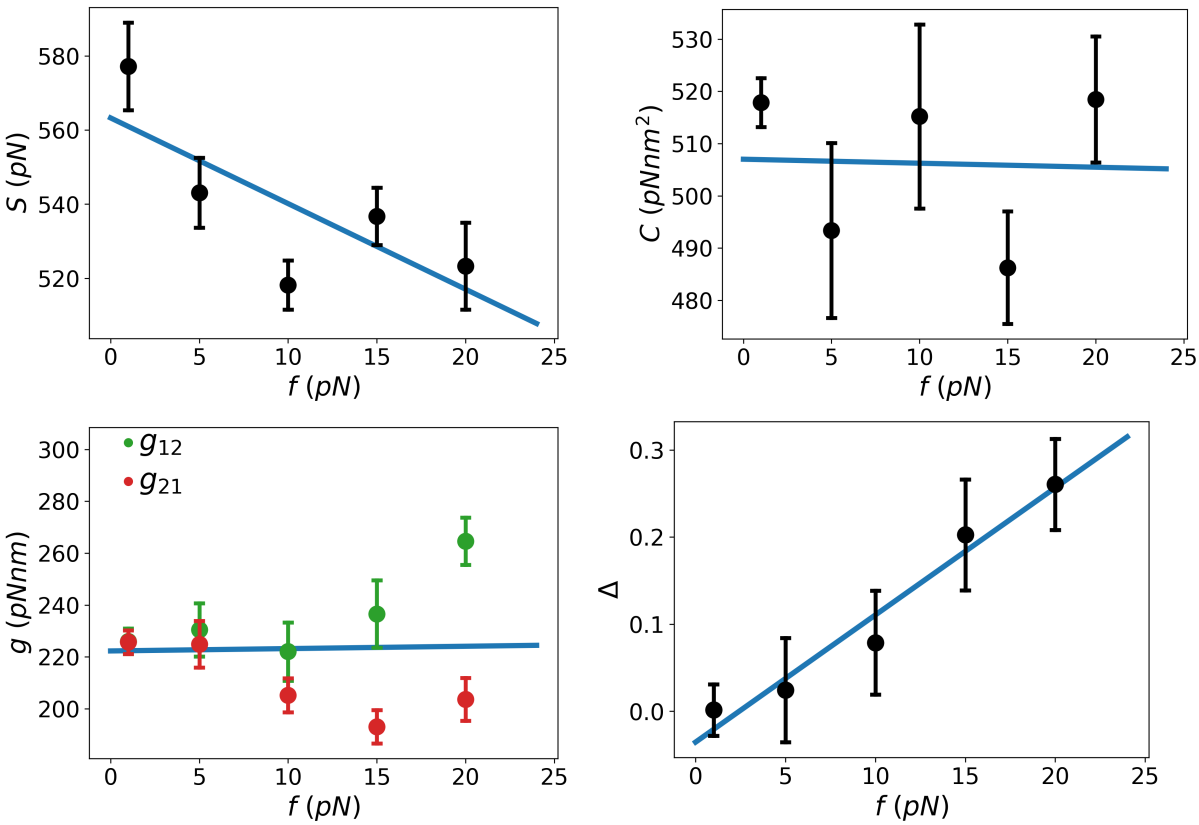

Figure S36: Force dependence of elastic parameters and constraint of seq3.

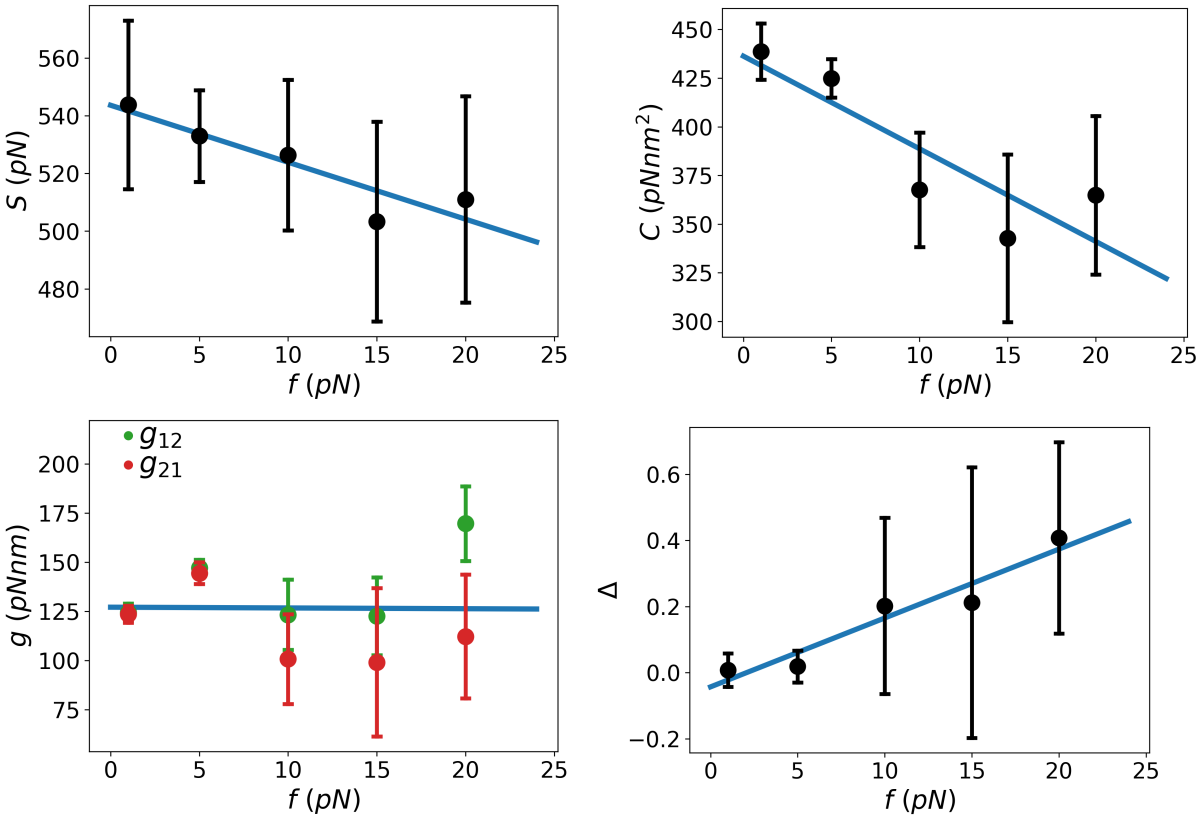

Figure S37: Force dependence of elastic parameters and constraint of seq4.

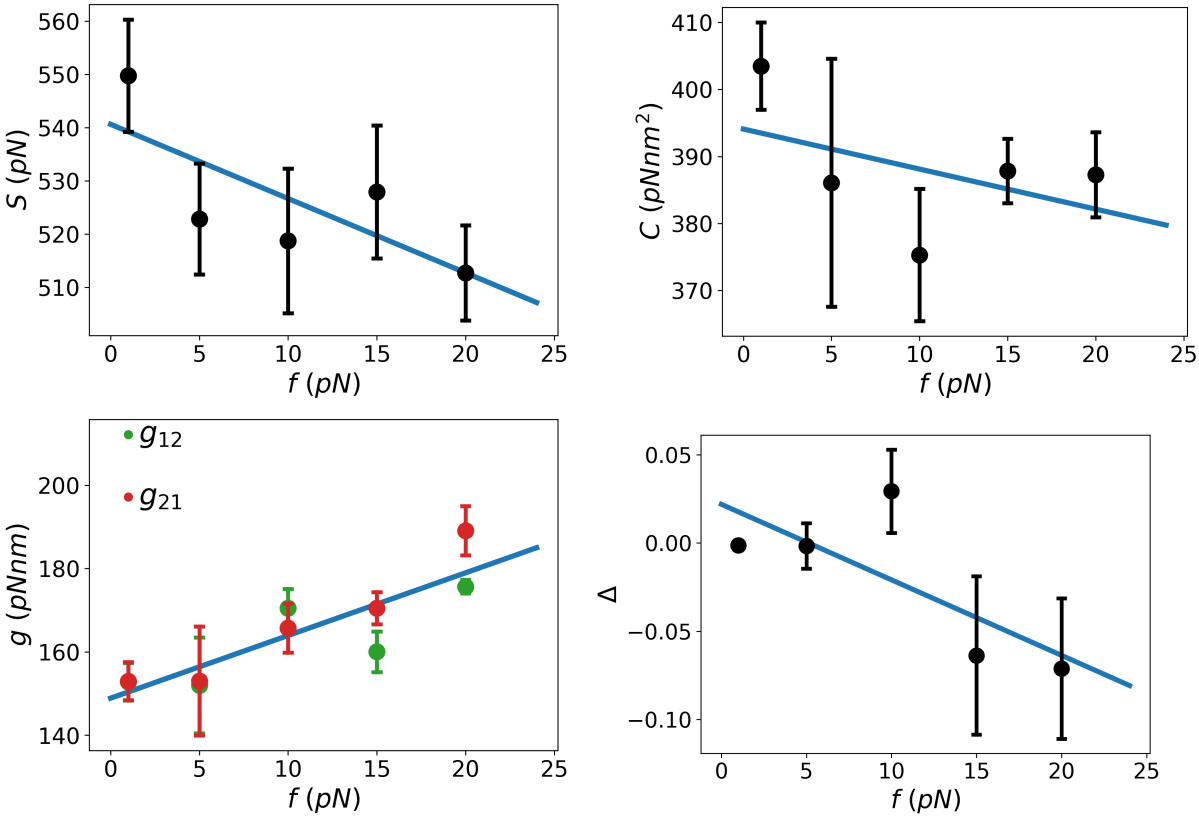

Figure S38: Force dependence of elastic parameters and constraint of RNAall.